Tectonophysics 639 (2015) 1–22

Contents lists available at ScienceDirect

Tectonophysics

journal homepage: www.elsevier.com/locate/tecto

Neogene erosion of the Andean Cordillera in the flat-slab segment as indicated by petrography and whole-rock geochemistry from the Manantiales Foreland Basin (32°–32°30′S)

Pablo Alarcón [a], Luisa Pinto [b,*]

[a] Universidad de Concepción, Facultad de Ciencias Químicas, Departamento Ciencias de la Tierra, Edmundo Larenas 129, Casilla 160-C, Concepción, Chile
[b] Departamento de Geología, Facultad de Ciencias Físicas y Matemáticas, Universidad de Chile, Plaza Ercilla 803, Casilla 13518, Correo 21, Santiago, Chile

ARTICLE INFO

Article history:
Received 1 April 2014
Received in revised form 23 October 2014
Accepted 2 November 2014
Available online 8 November 2014

Keywords:
Andes
Flat-slab
Manantiales Foreland Basin
Provenance
Sedimentary rocks
Whole-rock geochemistry

ABSTRACT

The Miocene Manantiales Foreland Basin is defined as a thick succession of sedimentary rocks belonging to the Chinches Formation in the Frontal Cordillera between 32°S and 32°30′°S, located over the flat-slab segment of the Andean Cordillera. It has been interpreted as a foreland basin that mainly received contributions from several mountain ranges such as the Principal Cordillera and Frontal Cordillera to the west. In this paper, we present a detailed study of its provenance based on the petrography and whole-rock geochemistry of sedimentary rocks from the Chinches Formation. Our results indicate that the Manantiales Basin was fed by igneous provinces in the hinterland that contain sub-alkaline intermediate rocks (andesitic) and acidic rocks (dacitic to rhyodacitic and granitic) arranged in a clear stratigraphic progression. These signatures may be assigned to Cenozoic rocks (Farellones Formation) in the Principal Cordillera and Permo-Triassic (Choiyoi Group) in the Frontal Cordillera. In contrast to a previous result, we found a continuous geochemical trend in the Chinches Formation between ca. 19 and 10 Ma opposing the idea of a tectonic repetition in the sedimentary succession.

1. Introduction

The South American Andes from Chile in the south to Panama in the north are well known to represent a long-lived continental arc system that produced intra-arc and foreland basins at least since Paleozoic times. Specifically, studies on the flat-slab zone of the Andes as well as to the south indicate that the blocks of the Principal Cordillera (Fig. 1a) in the Early Miocene were uplifted through a tectonic inversion (e.g., Charrier et al., 2002). This deformation probably propagated to the east during the Early to Late Miocene (e.g., Charrier et al., 2002; Fock et al., 2006; Giambiagi et al., 2003a; Muñoz Sáez et al., 2014) up to the Frontal Cordillera (Fig. 1b). This propagation developed thin- and thick-skinned thrust-fault-belts and foreland basins between the Principal Cordillera and the Frontal Cordillera. Thus, to understand the foreland basins it would help to establish the tectonic history of the subranges of the Andes at these latitudes. A provenance study of the sedimentary infill should reveal additional details about the uplifted tectonic bodies during the Miocene deformation.

In particular, the evolution of the Andes in the southern flat-slab at 32°–32°30′S will be better understood with an erosion history relating the Miocene syntectonic deposits, i.e. the Chinches Formation (Mirré, 1966) of the Manantiales Foreland Basin (e.g., Pérez, 1995; Jordan et al., 1996) with the uplifted blocks of the La Ramada Fold-thrust Belt (Cristallini et al., 1994). Coeval with the Chinches Formation to the west, in the Chilean side, the correlated Farellones Formation was deposited mainly between 25 and 12 Ma (Munizaga and Vicente, 1982) during the tectonic inversion of the Abanico Basin (Charrier et al., 2002; Jara and Charrier, 2014; Muñoz Sáez et al., 2014).

Sedimentological and provenance studies have already been conducted in the Chinches Formation (Jordan et al., 1996; Pérez, 1995, 2001). Jordan et al. (1996) considered the succession to be continuous and to comprise ~3.6 km of sedimentary rocks, whereas Pérez (1995, 2001) indicated that this succession has been duplicated due to faulting and has only one third of this thickness (1.3 km). This uncertainty regarding the stratigraphic succession causes a major problem when interpreting the true paleogeographic and tectonic significance and evolution of the basin, because origin interpretations of a continuous vs. a repeated sequence will be different with the blocks rose at each stage of tectonic uplift. Structural studies at this latitude based on a duplicated succession led to uncertain timing stages of deformation, being suggested uplift ages for the Frontal Cordillera to the Pliocene (Ramos et al., 1996a) and Middle Miocene (Cristallini et al., 1994; Cristallini and Ramos, 2000; Pérez, 2001). Additionally, continuous sedimentation according to data from Jordan et al. (1996) suggests that 3000 m of sediments was deposited in ca. 9 Ma, implying an overall sedimentation rate of ~333 m/Ma, similar to the high rate for this kind of basin (50–

* Corresponding author. Tel.: +56 229784106; fax: +56 2 26963050.
E-mail address: lpinto@ing.uchile.cl (L. Pinto).

http://dx.doi.org/10.1016/j.tecto.2014.11.001
0040-1951/

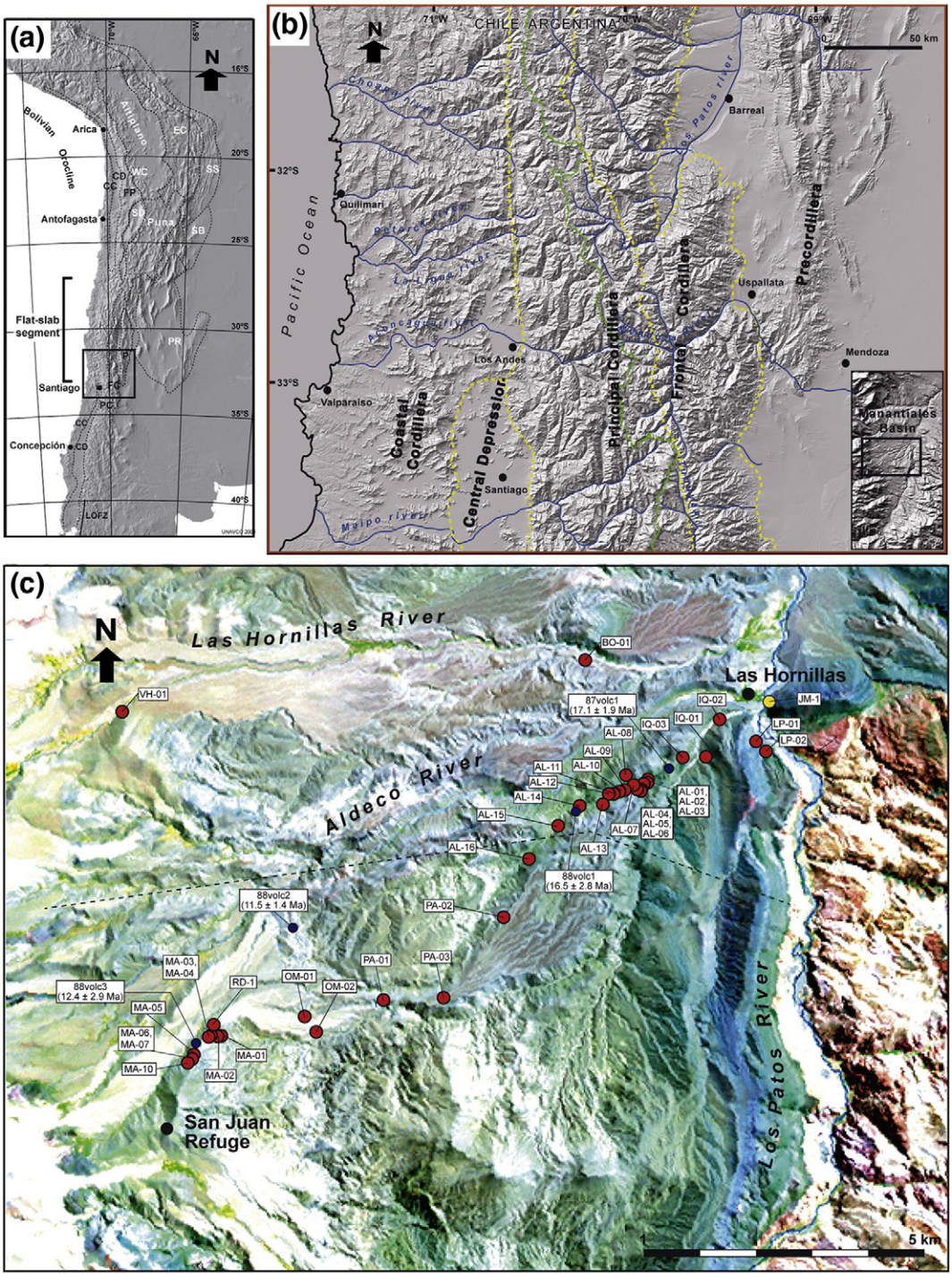

Fig. 1. a) Digital elevation model (DEM) of the Andes between 16°S and 40°S with an indication of the main geographical, tectonic and morphostructural features. Location of Fig. 1b is shown. b) Regional scale DEM with tectonic and morphological global features (marked by yellow segmented lines), where the study area is located (box). c) LANDSAT-TM image showing the location of the samples. Four dated samples (fission-track in zircons from tuffs) from Jordan et al. (1996) are located. Abbreviations: CC, Coastal Cordillera; CD, Central Depression; EC, Eastern Cordillera; FC, Frontal Cordillera; FP, Forearc Precordillera (western flank of the Altiplano and, further south, Sierra de Moreno); LOFZ, Liquiñe-Ofqui Fault Zone; P, Precordillera in Argentina; PC, Principal Cordillera; PR, Pampean Ranges; SB, Santa Barbara System; SD, Salars Depression; SS, Subandean Sierras; WC, Western Cordillera.

1000 m/Ma on average; 200–500 m/Ma for foreland basins of the southern Himalaya: Einsele, 1992).

Moreover, based on the petrology of sedimentary clasts and sandstone petrography, Pérez (2001) and Jordan et al. (1996) showed in general terms that the source rocks of the Manantiales Basin were Mesozoic sedimentary, and Paleozoic and Cenozoic volcanic rocks from the Principal Cordillera and Frontal Cordillera. However, they did not identify variations in the contribution to the basin nor the geochemical character of the igneous sources. These data are essential to understand the contribution of volcanic units from the Principal Cordillera, which crop out widely, but whose erosion has not been clearly identified in the foreland basins. The preservation of foreland basins with a supply from magmatic arcs and variations in contribution, such as the Manantiales Basin, are rare in the world, so that it is even more important to establish its provenance and tectonic implications.

There are several studies which provenance analysis of the sedimentary rocks helped to establish the erosional histories and to solve stratigraphic problems using the correlation of the sediments to discern their

sources (e.g., Mange and Maurer, 1992; Mange and Morton, 2007; Parfenoff et al., 1970; Pinto et al., 2007). The aim of a provenance analysis is to discover the nature of the sediment source rocks, from the type of rock to their specific affinities (e.g., Gabo et al., 2009; Krawinkel et al., 1999; Kutterolf et al., 2008; Lee, 2002; Morton, 1991; Pettijohn et al., 1987; Yang et al., 2011). The methods are diverse, ranging from the petrology of sedimentary clasts and sandstone petrography to detailed studies of the overall chemical composition of the sedimentary rocks (e.g., Arribas et al., 2007; Bhatia, 1983; Pinto et al., 2004; Roser and Korsch, 1986) and specific detrital heavy minerals (e.g., Krawinkel et al., 1999; Pinto et al., 2004, 2007; Rodríguez et al., 2012). Furthermore, researchers can obtain a complete understanding of the source rocks using a combination of several methods including the sediment geochemistry, which is strongly characterized by the rock-forming minerals derived from an igneous origin (e.g., Bhatia, 1983; Moine, 1974; Pettijohn et al., 1972; Pinto et al., 2004, 2007; Rodríguez et al., 2012). Among these studies, several concentrate on the major and trace element chemistry, the latter proving to be a useful tool for the discrimination and characterization of the source rock (e.g., Bhatia, 1983; Floyd and Leveridge, 1987; Kutterolf et al., 2008; Lee, 2002; Nesbitt and Young, 1984; Pettijohn et al., 1972; Potter, 1978; Roser and Korsch, 1986).

In this contribution, therefore, we present a detailed sediment geochemical study of the Chinches Formation that can be used to establish an erosional model and its tectonic implication as related to the uplifted blocks during the Miocene Andean orogeny in the southern flat-slab segment. We used a provenance method based on the sandstone petrography and whole-rock major and trace element geochemistry of the Chinches Formation. Through it, we provide new evidence to establish a detailed erosional history of the uplifted blocks in the Principal Cordillera and Frontal Cordillera at 32°-32°30'S, by recording a progression of igneous sources of the sedimentary succession in the Manantiales Basin.

2. Tectonic setting

The Andes Cordillera is a continuous mountain range along the western margin of South America that was formed by the subduction of the oceanic plate beneath the continental margin (Fig. 1a) (Dewey and Bird, 1970). This mountain range varies significantly and systematically along its strike (~9,000 km) in terms of topography, morphology, tectonics, the distribution of basins, volcanism, subduction geometry, crustal thickness, lithospheric structure and geological history (e.g., Baranzangi and Isacks, 1976; Cahill and Isacks, 1992; Gutscher, 2002; Jordan et al., 1983; Mpodozis and Ramos, 1989; Tassara and Yáñez, 1996). Subduction along this margin does not have a homogeneous dip. Between ~27°S and 33°S, the so-called flat-slab segment has a very low subduction dip angle (~5–10°) (Fig. 1a). To the north and to the south, the dip angle increases to ~30°, being constant with depth (e.g., Baranzangi and Isacks, 1976; Cahill and Isacks, 1992; Gutscher et al., 2000). The southern boundary of the flat-slab segment has an approximately east to west orientation (N80°E) (e.g., Kley et al., 1999). Extrapolating this trend and considering the morphostructural features, the southern flat-slab boundary can be traced to ~33°S on the Chilean side and ~32.5°S on the Argentinean side of the Andes (Fig. 1a).

The morphotectonic model for the flat-slab segment postulates that the region would have evolved gradually from a subduction angle of 30° to its current configuration mainly from the late Early Miocene to Pliocene (17–6 Ma) (e.g., Bissig et al., 2001, 2002, 2003). As a result of this process, volcanism would have ceased at ca. 6 Ma (e.g., Kay and Mpodozis, 2002). It has been suggested that the subduction of the Juan Fernández Ridge triggered the flat-slab configuration at the continental margin by buoyancy (e.g., Gutscher et al., 2000; Yáñez et al., 2001). Coeval with the tilting of the slab, crustal thickening occurred and the deformation spread eastward through thick-skinned faulting in the Precambrian-Paleozoic basement (Jordan et al., 1983).

The Cenozoic tectonics in this segment produced a steep morphology with the development of the Coastal Cordillera, Principal Cordillera, Frontal Cordillera, Precordillera, and Sierras Pampeanas between the forearc and the foreland region (Ramos et al., 2002) (Fig. 1). However, the chronology of the development of these morphologic features has not been established in detail. Ramos et al. (1996a) proposed that the deformation occurred during the last ca. 22 million years.

The eastern side of the Principal Cordillera in the southernmost flat-slab segment is characterized by the presence of the La Ramada Fold-and-thrust Belt (LRFTB, Figs. 1 and 2) (e.g., Cristallini et al., 1994; Ramos et al., 1996a, 1996b, 2002). This mega-structure at first had a thin-skinned character and would have been formed during the Early Miocene (e.g., Cristallini and Ramos, 2000; Jordan et al., 1996; Ramos et al., 1996b) or before (Cristallini et al., 1994). The LRFTB at second developed a main thick-skinned character formed by the inversion of an Upper Triassic extensional basin in the Middle Miocene (ca. 14–12 Ma) (Cristallini and Ramos, 2000; Ramos et al., 1996a, 1996b). At these latitudes, shortening until the Late Miocene (9 Ma) occurred mainly in the Precordillera, while southward, in the Aconcagua segment (33°–34°S) where there are no Precordillera and Pampean Ranges, shortening occurred in the Principal Cordillera (Ramos et al., 1996a, 1996b) thereby developing the mainly thin-skinned Aconcagua Fold-and-thrust Belt, the thick-skinned character being restricted to the west (Giambiagi et al., 2003a). Therefore, the subduction geometry that defines the flat-slab segment north to 33°S and the normal segment south to 33°S played a fundamental role in the tectonic evolution of both segments (Charrier et al., 2007; Giambiagi et al., 2003a). Associated with the evolution of the fold-and-thrust belts, syntectonic basins such as the Manantiales and Alto Tunuyán Basins developed in the foreland region and were well preserved between uplifted blocks (Fig. 2) (e.g., Giambiagi et al., 2003a, 2003b; Jordan et al., 1996; Pérez, 1995, 2001).

3. Manantiales Basin

The Manantiales Basin (31°45′–32°30′S, Figs. 1 and 2) was defined by Pérez (1995) as an Andean foreland basin cropping out between blocks of the Frontal Cordillera to the southeast of Barreal, Argentina (Fig. 1b). It is located in the Central Andes (e.g., Aubouin, 1973) in the southern part of the flat-slab subduction segment, between 32° and 33°S (Ramos et al., 1996a). This foreland basin is associated with the LRFTB and is parallel to the strike of the structures (~ NNW) (Jordan et al., 1996; Ramos, 1999; Ramos et al., 1996b). The development of this basin took place east of the Principal Cordillera during Miocene times, due to the eastward propagation of deformation (Cristallini et al., 1994). The basin is N–S oriented and is approximately 65 km by 18 km (Jordan et al., 1996; Pérez, 1995, 2001). At the present western margin of the basin, there is an east-vergent thrust fault (Espinacito Fault) corresponding to the easternmost main fault of the LRFTB (Álvarez and Pérez, 1993; Pérez, 1995).

The Manantiales Basin contains the Miocene Chinches Formation. This formation was defined by Mirré (1966) and mainly consists of clastic sedimentary rocks ranging from shales to conglomerates, with interbedded volcanic rocks (andesitic breccia and tuffs). The sedimentary rocks correspond to a coarsening-upward succession, from mainly sandstones at the base to conglomerates at the top (Jordan et al., 1996; Pérez, 1995, 2001). The sediments were mainly deposited in braided fluvial channel and floodplain environments, with lacustrine and alluvial fan sediments towards the top (Fig. 6 in Jordan et al., 1996). Jordan et al. (1996) established that the paleocurrent directions in the Chinches Formation were oriented from west to east.

The potential source rocks for the basin fill are located in the Principal Cordillera and the Frontal Cordillera to the west (Figs. 2 and 3). The main units correspond to rhyolitic and rhyodacitic volcanic rocks from

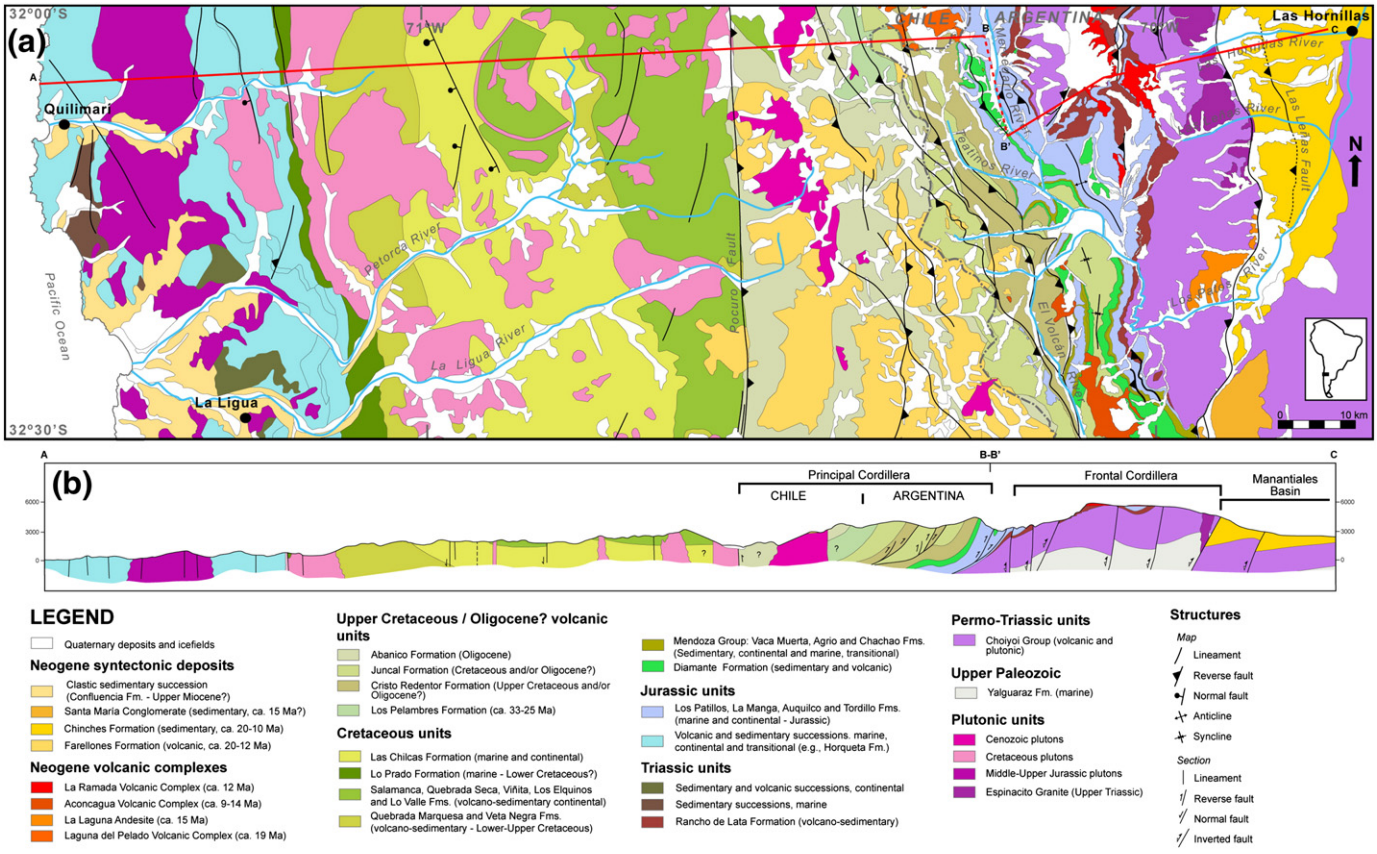

Fig. 2. Regional geological map (a) and section (b) indicating the geological units in Chile and Argentina between 32° and 32°30'S, between the Chilean littoral and the Manantiales Basin. The principal morphostructural units are indicated on the section. Based on Rivano et al. (1993), Cristallini and Cangini (1993), Cristallini et al. (1994), Pérez (1995, 2001), Ramos et al. (1996b), Cristallini and Ramos (2000), Sernageomin (2003), Mpodozis et al. (2009) and Jara and Charrier (2011, 2014).

the Choiyoi Group (Permian to Early Triassic age) (e.g., Mirré, 1966; Stipanicic et al., 1968; Martínez, 2005; Martínez and Giambiagi, 2010), Mesozoic sedimentary rocks of marine and continental character (Mendoza Group, and Tordillo, Auquilco, La Manga, Los Patillos, Rancho de Lata and Diamante Formations) (Ramos et al., 1996b), mainly intermediate volcanic rocks (andesites and andesitic volcaniclastic rocks) of the Abanico (Oligocene), Farellones (Miocene), Juncal and Cristo Redentor (Mesozoic or Cenozoic?) Formations (e.g., Rivano et al., 1993; Cristallini and Cangini, 1993; Ramos et al., 1996b; Cristallini and Ramos, 2000; Charrier et al., 2002, 2005, 2007; Mpodozis et al., 2009; Jara and Charrier, 2011, 2014), and correlated units such as the Laguna del Pelado Volcanic Complex, La Ramada Volcanic Complex, and the La Laguna subvolcanic andesitic body (equivalent to the Farellones Formation). According to Pérez (1995), different ranges in the Principal Cordillera were uplifted from west to east, all located to the west of the Chinches Formation outcrops, finishing with the Cordillera del Tigre to the east (Fig. 10 in Pérez, 2001). This erosion would be a normal progression of the fold-and-thrust-belt type of deformation (Cristallini and Ramos, 2000; Cristallini et al., 1994; Pérez, 1995).

4. Methods

We collected 38 samples in the Chinches Formation: 36 from sedimentary rocks and two igneous samples (Fig. 4 and Table 1).

The two igneous samples (JM-1 and RD-1), one intermediate and the other acidic in composition, were collected on the assumption that these end-members are representative of the suite of igneous samples of the region, and we compared the chemistry of the studied sedimentary rocks with them. Sample JM-1 corresponds to a volcanic andesitic breccia taken from the lower unit at Las Hornillas (Figs. 1 and 4) (Pérez, 1995, 2001). Sample RD-1 corresponds to a clast probably coming from the Espinacito Granite picked up at the top of the Chinches Formation.

We made, at the University of Chile, petrographic thin sections of 21 representative samples of sandstones to determine the type of rock and the mineral composition under the microscope (Table 2). The thin sections were described and a modal count was done by the method of Gazzi-Dickinson (Dickinson, 1970; Ingersoll et al., 1984). Three hundred points were counted per sample and the data were plotted on diagrams proposed by Folk et al. (1970) and modified by Dickinson et al. (1983) to classify the type of sandstone and discriminate the tectonic setting (Table 2).

The samples used in the geochemical analysis (36 samples, Table 3) were prepared in the Geology Department of the University of Chile. The samples were pulverized in an agate mortar and a coarse pulp was obtained. We performed whole-rock geochemical analyses on all of the samples (Table 3) using a combination of packages; lithium metaborate/tetraborate fusion ICP whole rock (Code 4B) and trace element ICP/MS (Code 4B2) at Actlabs, Ontario, Canada. The fused sample was diluted and analyzed by Perkin Elmer Sciex ELAN 6000, 6100 or 9000 ICP/MS. Three blanks and five controls (three before the sample group and two after) were analyzed per group of samples. The duplicates were fused and analyzed for every 15 samples. The instrument was recalibrated for every 40 samples.

The whole-rock geochemical data were used to characterize the essential aspects of the Chinches Formation samples, using discrimination diagrams and spider diagrams, in order to discriminate the tectonic environment and the chemical signatures of the igneous source rocks that

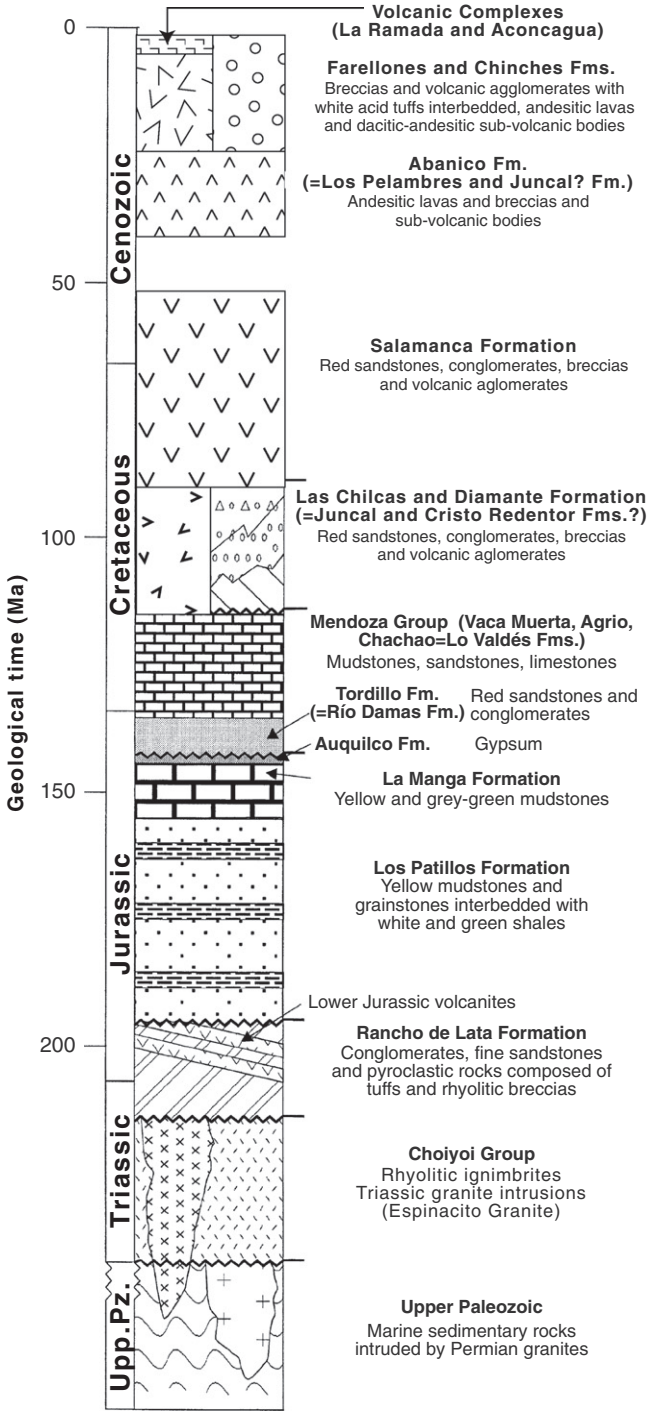

Fig. 3. Stratigraphic column of the regional units on the eastern border of the Principal Cordillera between 32° and 33°S (modified from Cristallini and Ramos, 2000), which are potential sediment sources of the Chinches Formation.

contributed to the Manantiales Basin (e.g., Pinto et al., 2007). We present a geochemical analysis of the Chinches Formation based on the major and trace elements data by: a) discriminating between the data that retain an igneous signature and those in which the sedimentary processes (e.g., transport, sedimentation, lithification) have hidden the igneous character of the sources, b) characterizing the geochemical signatures and trends of the sedimentary rocks, c) conducting a global tectonic setting discrimination of the sources, and d) characterizing the geochemical signatures of the igneous sources.

The samples from the Chinches Formation are plotted according to their stratigraphic position in three informal units: a lower unit, middle unit and upper unit (Table 1 and Fig. 4).

The sedimentary rocks from the Chinches Formation have a red appearance given by Fe-oxides dispersed as a fine-grained pigment. However, this is not quantitatively abundant enough to strongly affect the total Fe composition in the samples (Pettijohn et al., 1972). When the sediments were rich in carbonate, the analyses were recalculated to be $CaCO_3$-free (see below). The data were recalculated to be 100% volatile-free.

In addition, we compiled all of the available published geochemical data from potential source rocks (e.g., Fuentes, 2004; Levi, 2010; Montecinos, 2008; Pérez, 1995; Pinto et al., in preparation; Ramos et al., 1996b; Vergara and Nyström, 1996; Vergara et al., 1993) to compare them to the geochemistry of our samples.

5. Results

Below, we show the results from the petrographic (Table 2) and geochemical (Table 3) analyses carried out on the studied rocks.

5.1. Petrography

The petrography of the samples, graphed in the Q–F–L diagram (Folk et al., 1970) (Fig. 5a) indicates that they mainly correspond to lithic feldsarenite (62%), and secondary feldsarenite (19%) and feldespathic lithoarenite (14%), with minor lithoarenite (5%) (Table 2). The main components are plagioclase (15–79.3%), volcanic lithics (0–64%) and quartz (1.0–51.3%). K-feldspar is scarce (0.3–15.3%). The P/Ft ratio (P: plagioclase, Ft: total feldspar) presents high values from 0.6 to 1.0, indicating a significant supply from volcanic sources (Dickinson, 1970). The metamorphic and sedimentary lithics are present in trace quantities (<1%). The cement is calcareous (1–37%) with a minor percentage of Fe–Ti oxides (0–6%).

5.2. Major element chemistry

5.2.1. CaO vs. LOI

To identify the amount of carbonate (cement or carbonate clasts) in the samples, we compared the weight percent of CaO and LOI (Lost on Ignition) (Fig. 6a, b). There is a linear relationship between CaO and LOI wt.% (Fig. 6a, b) and the CaO wt.% is slightly above the average for sedimentary rocks, reflecting a significant contribution from igneous rocks (Fig. 6). By reducing the LOI by a percentage proportional to the CO_2 in the calcite formula (7.8 wt.% LOI vs. 10 wt.% CaO) (Fig. 6a), we eliminated the excess of CaO associated with calcite in order to more clearly discriminate the signatures of the igneous rock sources. Then, we set all of the oxides back to 100%, which eliminated the presence of calcite as cement or clasts of carbonate rocks.

5.2.2. Chemostratigraphy based on major elements

The chemostratigraphy (stratigraphic chemical variations of samples in a sequence, e.g. Fig. 7), as reflected in its patterns and in specific chemical breaks, may provide information about changes in the source rocks (Floyd and Leveridge, 1987). We used the whole-rock geochemistry without recalculating Ca to explore the general signatures of the samples. The chemostratigraphy of the major elements in the Chinches Formation (Fig. 7) shows that the lower unit is relatively homogeneous in SiO_2, Al_2O_3, K_2O and Na_2O, whereas the middle and upper units show a greater variation of these elements (Fig. 7). In addition, the succession displays a good correlation between Fe and Mg except for some samples (LP-01, IQ-03, MA-07 and MA-10, Fig. 7), suggesting that these elements are controlled by ferromagnesian minerals. Furthermore, there is a correlation between Fe^{+3} and Ti (except AL-16, BO-01 and PA-02, Fig. 7), indicating that their abundance is controlled by Fe–Ti oxides.

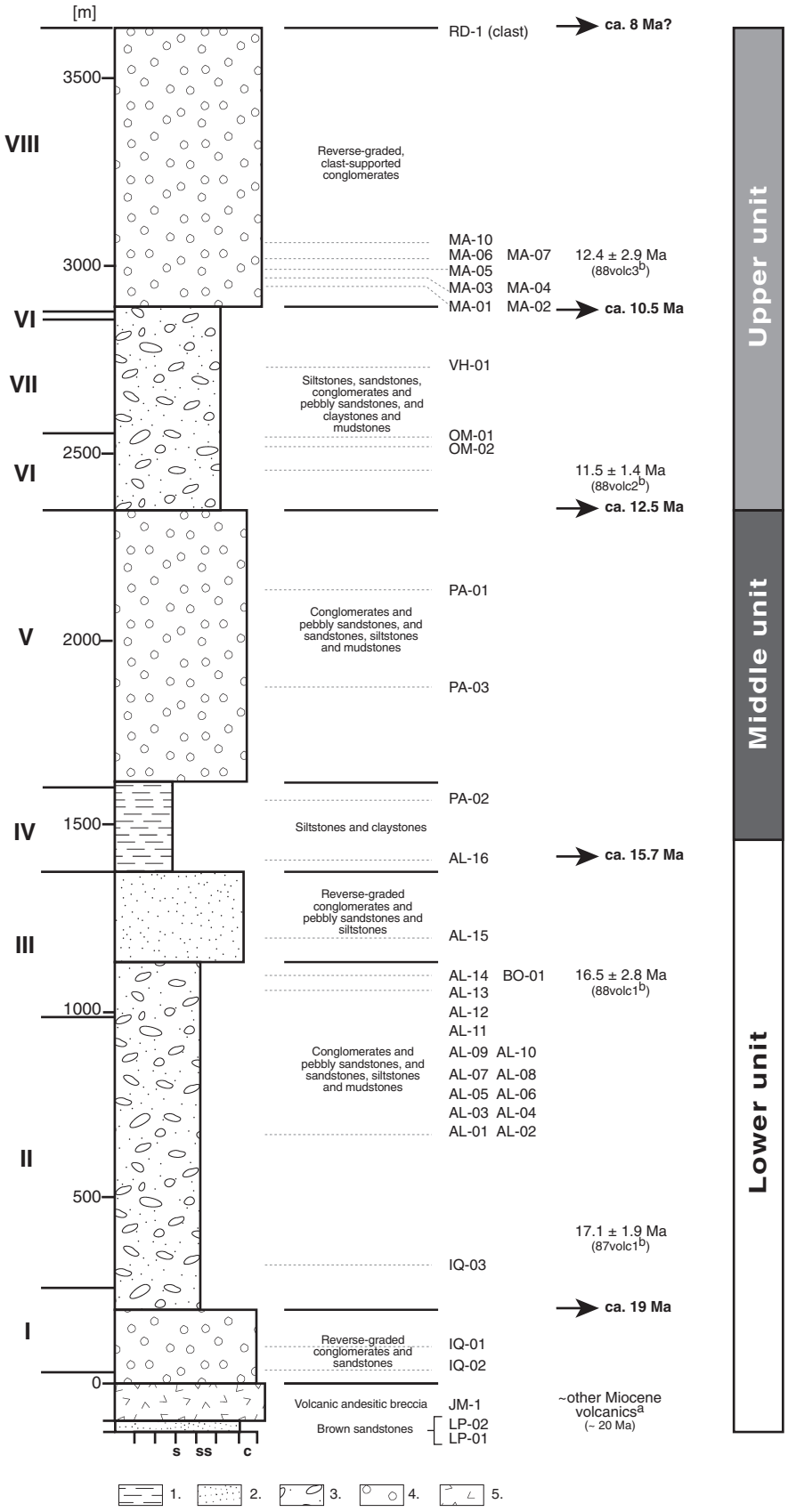

Fig. 4. Schematic column of the Chinches Formation based on Jordan et al. (1996), showing the position of the analyzed samples and informal units used in this study. 'a': age correlation given by Pérez (2001), 'b': age data (fission-track on zircons from tuffs) given by Jordan et al. (1996). The estimated ages in bold are based on the magnetostratigraphy study of Jordan et al. (1996). The Roman numerals I to VIII indicate the facies groups identified by Jordan et al. (1996). Symbols: Grain-size: s, siltstone; ss, sandstone; c, conglomerate. Lithologies: 1. Limestones and sandstones, 2. Sandstones, 3. Conglomerates, sandstones and siltstones, 4. Conglomerates, 5. Volcanic breccia.

Table 1
Location of sedimentary samples from the Chinches Formation.

Sample	Rock kind	Clast abundance	Informal units	Locality	Longitude W	Latitude S	Altitude
LP-02	Sandstone	–	Lower unit	Los Patos River	69°45′29″	32°13′31″	2096
LP-01	Sandstone	–	Lower unit	Los Patos River	69°45′36″	32°13′25″	2074
JM-1	Volcanic breccia	–	Lower unit	Las Hornillas	69°45′27″	32°13′2″	2070
IQ-02	Sandstone	–	Lower unit	Las Hornillas	69°45′58"	32°1′55"	2092
IQ-01	Sandstone	–	Lower unit	Las Hornillas	69°46′17"	32°2′16"	2143
IQ-03	Sandstone	–	Lower unit	Las Hornillas	69°46′23"	32°2′17″	2141
AL-01	Sandstone	–	Lower unit	Las Hornillas	69°46′47″	32°2′29″	2164
AL-02	Sandstone	–	Lower unit	Las Hornillas	69°46′48″	32°2′31″	2179
AL-03	Sandstone	++	Lower unit	Las Hornillas	69°46′50″	32°2′32″	2172
AL-04	Sandstone	+	Lower unit	Las Hornillas	69°46′52″	32°2′35″	2173
AL-05	Sandstone	–	Lower unit	Las Hornillas	69°46′52″	32°2′36″	1186
AL-06	Sandstone	–	Lower unit	Las Hornillas	69°46′55″	32°2′35″	2187
AL-07	Sandstone	–	Lower unit	Las Hornillas	69°46′57″	32°2′32″	2187
AL-08	Sandstone	–	Lower unit	Las Hornillas	69°46′2″	32°2′27″	2098
AL-09	Sandstone	–	Lower unit	Las Hornillas	69°47′3″	32°2′35″	2232
AL-10	Sandstone	–	Lower unit	Las Hornillas	69°47′7″	32°2′36″	2234
AL-11	Sandstone	–	Lower unit	Aldeco River	69°47′11″	32°2′37″	2201
AL-12	Sandstone	–	Lower unit	Aldeco River	69°47′14″	32°2′38″	2201
AL-13	Sandstone	+	Lower unit	Aldeco River	69°47′18″	32°2′44″	2215
AL-14	Sandstone	–	Lower unit	Aldeco River	69°47′34″	32°2′45″	2230
BO-01	Sandstone	–	Lower unit	Las Hornillas River	69°47′3″	32°12′3″	2294
AL-15	Sandstone	–	Lower unit	Aldeco River	69°47′49″	32°2′56″	2280
AL-16	Sandstone	–	Lower unit	Aldeco River	69°48′9″	32°3′15″	2306
PA-02	Sandstone	++	Middle unit	Manantiales Pampa	69°48′27″	32°3′49″	2501
PA-03	Sandstone	+	Middle unit	Manantiales Pampa	32°4′36″	69°49′8″	2637
PA-01	Sandstone	+++	Middle unit	Manantiales Pampa	69°49′49″	32°4′37″	2307
OM-02	Sandstone	++	Upper unit	San Juan Refuge	32°4′45″	69°50′3″	2770
OM-01	Sandstone	++	Upper unit	San Juan Refuge	32°4′46″	69°50′43″	2786
VH-01	Sandstone	+	Upper unit	Las Hornillas River	69°52′50″	32°13′5″	2930
MA-01	Sandstone	–	Upper unit	Manantiales	69°51′40″	32°4′57″	2920
MA-02	Sandstone	+++	Upper unit	Manantiales	69°51′43″	32°4′57″	2970
MA-03	Sandstone	+++	Upper unit	San Juan Refuge	69°51′47″	32°4′57″	3008
MA-04	Sandstone	+++	Upper unit	San Juan Refuge	69°51′49″	32°4′57″	3015
MA-05	Sandstone	–	Upper unit	San Juan Refuge	69°52′00″	32°5′8″	3064
MA-06	Sandstone	–	Upper unit	San Juan Refuge	69°52′00″	32°5′10″	3044
MA-07	Sandstone	++	Upper unit	San Juan Refuge	69°52′00″	32°5′10″	3044
MA-10	Sandstone	+++	Upper unit	San Juan Refuge	69°52′3″	32°5′12″	3079
RD-1	Granitic clast	–	Upper unit	San Juan Refuge	69°51′4″	32°4′49″	3030

Symbols: '–' absent, '+' low, '++', moderate, and '+++' high quantities.

There are some samples with anomalous concentrations of certain elements with respect to their neighboring samples, for example, AL-15 and AL-16 in CaO (~15 wt.%) and TiO_2 (~0.9 wt.%), AL-16 and BO-01 in MgO (~3 wt.%), LP-02 in K_2O (~4.5 wt.%) and MA-06 and MA-07 in Na_2O (~3.3 wt.%).

5.2.3. Weathering of the rocks

Sedimentary rocks are potentially affected by alteration processes, which modify both the minerals and the rock chemistry (e.g., Fedo et al., 1995; Lee, 2002; McLennan et al., 2004; Nesbitt and Young, 1982, 1984; Yang et al., 2011). Nesbitt and Young (1982) introduced the "Chemical Index of Alteration" (CIA) to quantify the degree of alteration (Fig. 8).

Sedimentary rocks from the Chinches Formation have characteristics of fresh or slightly weathered rocks, as shown in the Al_2O_3–CaO–Na_2O + K_2O diagram (Fig. 8) (Nesbitt and Young, 1984), where CaO^* is defined as CaO in silicates. In this same diagram, the CIA values are shown as ranging between 55.3 and 74.0 (61.5 on average) (Fig. 8). The maturity ratios are low and range between 2.7 and 6.3 (4.6 on average), which allows us to refine our data in order to define the source rock characteristics.

5.2.4. Chemical classification

To classify our sandstones and to evaluate their grade of chemical maturity, we used the $\log(Na_2O/K_2O)$ vs. $\log(SiO_2/Al_2O_3)$ diagram of Pettijohn et al. (1972), as modified by Herron (1988). Most sedimentary rock samples show a low maturity (Fig. 9) reflected in the chemistry with abundant Al with respect to Si and abundant K with respect to Na, which is consistent with their syntectonic character (Jordan et al., 1996; Pérez, 1995, 2001). The maturity is slightly higher towards the upper unit (Fig. 9).

Most samples fall in the greywacke and litharenite fields, but the samples from the highest part of the upper unit fall in the arkose field (Fig. 9). According to hand specimen observations, samples that fall in the arkose domain present abundant quartz, due to an acidic source, which agrees with the chemical classification.

Samples MA-06 and MA-07 from the upper unit (Fig. 4) have a high Na_2O/K_2O ratio, low in SiO_2/Al_2O_3 (Fig. 9), showing a predominance of Na over K, and an Al-enrichment compared with the general trend of the other samples (Figs. 9 and 12) (see below). These characteristics of abundance in feldspathic and/or argylic minerals (see below) are different from the rest of the clastic samples, which are primarily composed of lithics.

5.3. Trace element chemistry

Discrimination diagrams based on trace elements used for sedimentary rocks become more sophisticated over the last decade (e.g., Hofer et al., 2013; Jorge et al., 2013). Those applied most often are multi-element plots (spider diagrams) and bi-dimensional graphs of elements or ratios. In this study, to begin with, we used chondrite-normalized diagrams (Pearce, 1983) based on data from Sun and McDonough (1989) (Fig. 10).

Table 2
Petrography of sedimentary samples from the Chinches Formation.

			Chinches formation																			
			Lower unit										Middle unit			Upper unit						
			LP-02	LP-01	IQ-02	IQ-01	IQ-03	AL-01	AL-05	AL-09	AL-14	AL-15	AL-16	PA-02	PA-03	PA-01	OM-02	OM-01	MA-01	MA-04	MA-06	MA-07	MA-10
Quartz	Monocrystalline	Ondulose	8.33	26.33	39.00	13.00	1.00	1.33	3.67	23.67	9.33	8.00	14.67	10.67	18.67	6.33	5.67	2.33	3.33	2.67	0.67	0.00	0.67
		Flash	1.67	3.67	3.33	3.00	0.00	0.00	2.33	1.67	0.00	3.33	3.33	0.33	4.67	1.00	1.00	5.00	0.33	10.00	0.33	0.67	1.33
	Polycrystalline	2–3 grains	3.33	0.67	0.67	0.00	0.00	0.33	0.33	1.00	0.00	0.00	0.33	1.33	0.33	0.00	0,00	0.33	0.00	0.00	0.00	0.00	0.00
		4–5 grains	7.00	1.67	1.00	1.33	0.33	0.33	1.33	4.33	1.67	1.00	0.00	1.33	1.00	2.67	2,33	2.00	0.67	0.33	0.00	0.00	0.67
		More than 5 grains	19.33	4.67	7.33	1.67	4.33	9.33	8.00	20.67	7.67	3.00	20.00	21.00	12.00	9.00	14.67	8.33	1.00	17.00	0.00	2.00	14.67
Feldspar		Plagioclase	16.33	15.00	21.33	15.67	56.00	53.00	3.,67	20.00	44.00	40.33	21.33	29.00	22.00	49.00	47.33	63.00	53.33	46.00	79.00	79.33	60.33
		Microcline	0.33	0.00	0.00	0.00	0.00	0.00	0.00	0.00	0.00	0.67	0.33	0.00	0.33	0.67	0.00	0.33	0.33	0.33	0.00	0.00	0.00
		Orthoclase	4.33	3.67	8.67	0.67	1.33	033	0.33	8.33	1.33	0.67	15.33	10.33	11.33	5.33	3.00	3.67	0.67	0.67	2.00	0.67	1.67
Rock fragments	Volcanic rock fragments	With seriate textures	3.33	0.67	0.67	9.67	4.67	2.67	6.67	0.67	1.67	15.00	4.00	3.67	4.33	1.67	4.67	0.33	15.00	6.67	0.00	3.67	4.00
		With granular textures	1.67	1.33	1.33	13.33	4.00	6.00	10.00	1.00	7.67	0.33	6.33	2.00	1.67	1.33	0.00	0.33	0.67	1.67	0.00	0.00	2.00
		With microlithic textures	17.33	2.00	2.67	17.33	13.00	10.67	15.00	6.33	15.33	2.33	3.67	11.67	7.00	8.67	14.33	4.33	1.67	7.00	0.00	0.00	7.00
		With lathwork textures	10.33	3.67	4.33	23.00	15.00	13.67	12.33	9.00	8.33	25.00	4.33	3.33	8.67	4.67	5.00	0.67	20.33	3.33	0.00	2.00	1.00
		With vitric textures	1.67	0.00	1.00	0.67	0.00	0.67	1.00	0.00	0.67	0.00	1.67	1.67	2.33	1.00	0.00	0.00	0.00	1.33	0.00	0.00	0.67
	Methamorphic		0.00	0.00	0.00	0.00	0.00	0.00	0.00	0.00	0.00	0.00	0.00	1.00	0.00	0.00	0.00	0.00	0.00	0.00	0.00	0.00	0.00
	Sedimentary		0.00	0.00	0.00	0.33	0.00	0.00	0.33	0.00	0.67	0.33	0.33	0.67	0.00	0.33	0.00	0.00	0.00	0.67	0.00	0.00	0.33
	Pseudomatrix		0.00	0.00	0.00	0.00	0.00	0.00	0.00	0.00	0.00	0.00	0.00	0.00	0.00	0.00	0.00	0.00	0.00	0.00	0.00	0.00	0.00
	Altered lithics		0.00	0.00	0.00	0.00	0.00	0.00	0.00	0.00	0.00	0.00	0.00	0.00	0.00	0.00	0.00	0.00	0.00	0.00	0.00	0.00	0.00
Accessory minerals	Heavy minerals		1.67	30.67	2.67	0.33	0.33	1.67	0.00	2.33	1.33	0.00	3.67	1.00	2.00	4.67	1.00	0.33	1.00	1.00	1.33	1.00	4.00
	Miscellaneous and unidentified		3.33	5.67	5.67	0.00	0.00	0.00	0.00	1.00	0.00	0.00	0.67	0.67	3.33	3.67	1.00	6.33	1.33	0.67	16.67	10.67	0.67
	Phyllosilicates		0.00	0.33	0.33	0.00	0.00	0.00	0.00	0.00	0.33	0.00	0.00	0.33	0.33	0.00	0,00	2.67	0.33	0.67	0.00	0.00	1.00
Cements	Iron oxides		0.00	0.00	0.00	0.00	3.00	0.00	4.00	0.00	6.00	0.00	0.00	0.00	0.00	0.00	0.00	0.00	0.00	0.00	0.00	0.00	5.00
	Calcareous		10.00	20.00	28.00	12.00	1.00	5.00	17.00	19.00	4.00	10.00	23.00	37.00	23.00	16.00	33.00	11.00	14.00	30.00	8.00	17.00	20.00
	Argillaceous		0.00	0.00	0.00	0.00	0.00	0.00	0.00	0.00	0.00	0.00	0.00	0.00	0.00	0.00	0.00	0.00	0.00	0.00	0.00	0.00	0.00
Total			100	100	100	100	100	100	100	100	100	100	100	100	100	100	100	100	100	100	100	100	100
P/Ft			0.78	0.80	0.71	0.96	0.98	0.99	0.99	0.71	0.97	0.97	0.58	0.74	0.65	0.89	0.94	0.94	0.98	0.98	0.98	0.99	0.97
Q = total quartz			39.67	37.00	51.33	19.00	5.67	11.33	15.67	51,33	18.67	15.33	38.33	34.67	36.67	19.00	23.67	18.00	5.33	30.00	1.00	2.67	17.33
F = total feldspars			21.00	18.67	30.00	16.33	57.33	53.33	39.00	28.33	45.33	41.67	37.00	39.33	33.67	55.00	50.33	67.00	54.33	47.00	81.00	80.00	62.00
L = lithics + pollicrystalline quartz			34.33	7.67	10.00	64.33	36.67	33.67	45.33	17.00	34.33	43.00	20.33	24.00	24.00	17.67	24.00	5.67	37.67	20.67	0.00	5.67	15.00
Quartz 1 = ondulose + flash			10.00	30.00	42.33	16.00	1.00	1.33	6.00	25.33	9.33	11.33	18.00	11.00	23.33	7.33	6.67	7.33	3.67	12.67	1.00	0.67	2.00
Quartz 2 = polycrystalline			29.67	7.00	9.00	3.00	4.67	10.00	9.67	26.00	9.33	4.00	20.33	23.67	13.33	11.67	17.00	10.67	1.67	17.33	0.00	2.00	15.33
Acidic volcanic rocks fragments*			5.00	2.00	2.00	23.00	8.67	8.67	16.67	1.67	9.33	15.33	10.33	5.67	6.00	3.00	4.67	0.67	15.67	8.33	0.00	3.67	6.00
Basic volcanic rocks fragments**			27.67	5.67	7.00	40.33	28.00	24.33	27.33	15.33	23.67	27.33	8.00	15.00	15.67	13.33	19.33	5.00	22.00	10.33	0.00	2.00	8.00
Total volcanic lithics			34.33	7.67	10.00	64.00	36.67	33.67	45.00	17.00	33.67	42.67	20.00	22.33	24.00	17.33	24.00	5.67	37.67	20.00	0.00	5.67	14.67

*Acidic = volcanic rocks with seriate and granular textures; **Basic = volcanic rocks with microlithic and lathwork textures.

The rocks are fairly homogeneous and similar to the pattern of the upper crust (Rudnick and Gao, 2004). At the base of the lower unit, samples IQ-01, IQ-02, IQ-03, LP-01 and LP-02 have flat or slightly flatter patterns than the other samples (mainly LP-02) (Fig. 10). This is probably associated with the igneous intermediate character of these samples. The MA-06 and MA-07 samples show markedly different patterns in comparison to the rest of the samples, with a positive Eu anomaly ($Eu/Eu^* \sim 1.1$) and a steeper REE pattern ($La/Th \sim 13$). These samples have abundant Al_2O_3 and Na_2O with respect to the other samples, possibly showing the presence of clays such as montmorillonite.

The samples have similar concentrations of La (13.9–39.1), Ce (26.5–79.9), Nd (14.1–34.0) and ΣREE (73.5–186.7) (Table 3). In general, they are LREE-enriched and HREE-depleted, except for those samples from the lower and upper units mentioned above ($La_N/Yb_N = 5.9–13.2$, average = 8.4). Most of the samples show a negative Eu anomaly ($Eu/Eu^* = 0.6–0.9$, average = 0.7), except for samples LP-02, MA-06 and MA-07, which have a positive anomaly (Table 3).

6. Interpretation

6.1. Tectonic discrimination

The petrography date indicates that the overall tectonic setting of the samples, according to the discrimination diagram of Dickinson et al. (1983) (Fig. 5b), corresponds to a transitional arc. Some samples of the upper unit of the Chinches Formation (OM-01, MA-06, MA-07 and MA-10) are located in the basement uplift field. Also, concentrations of the most significant components from igneous sources were plotted in stratigraphic sequence in the following pairs: a) Total quartz and monocrystalline quartz, b) plagioclase and K-feldspar, and c) acidic and basic-intermediate lithics (Fig. 5c). In general terms, a tendency for a decrease in quartz and volcanic lithics and an increase in total feldspar are observed (Fig. 5). In most of the sequence basic-intermediate and acidic volcanic lithics have a direct relationship (Fig. 5c), indicating a common source area, while the total quartz and plagioclase present an inverse relationship, indicating different sources or source areas.

The tectonic setting of the succession was also evaluated using a discrimination diagram proposed by Roser and Korsch (1986) for greywackes, which plots the $\log(K_2O/Na_2O)$ vs. SiO_2 (Fig. 11), and has broad applications due to its independence of the grain size (e.g., Rollinson, 1993; Roser and Korsch, 1986; Kutterolf et al., 2008). This can be applied to sandstones as well as siltstones and mudstones (Roser and Korsch, 1986).

In this diagram our samples mainly fall in an active continental margin field (Figs. 4 and 11). Samples from the base of the lower unit (LP-01, LP-02, and IQ-03) have an affinity with the island arc field (Fig. 11), probably reflecting the abundance of ferromagnesian minerals in the source that could be related to a thinned continental crust. Samples from the highest part of the upper unit (MA-02, MA-03, MA-04, MA-05 and MA-10) have an affinity with the passive margin field, reflecting the abundance of light minerals such as quartz in the source. In particular, samples MA-06 and MA-07 plot separately from the other samples of this unit; this deviation is related to the very low K_2O concentration in these samples. Samples from the middle unit (PA-01, PA-02 and PA-03) have an intermediate trend from the active continental margin to the passive margin (Fig. 11), showing a mixture of rock sources between the samples from the lower and upper units.

6.2. Igneous character of the source

6.2.1. Igneous vs. sedimentary character

De La Roche (1968) introduced the (Al/3-K) vs. (Al/3-Na) diagram (Fig. 12) (modified by Moine, 1974), which can be used to discriminate between sedimentary and igneous domains, and to identify the compositional characteristics of the sedimentary rocks on the basis of the chemistry of specific rock-forming minerals. This diagram also depicts the chemical trends of the volcanic domain (basalts, andesites, dacites and rhyolites, both calc-alkaline and alkaline) as well as if the rocks have undergone little or strong alteration in elements such as Al, K, and Na (Fig. 12).

Twenty-five of the 36 samples from the Chinches Formation have igneous affinities. The remaining 11 samples (IQ-01, AL-05, AL-09, PA-01, PA-02, PA-03, MA-02, MA-03, MA-04, MA-05 and MA-10; Fig. 12), primarily belong to the middle and upper units of the Chinches Formation (Fig. 4) and fall within the sedimentary domain. The affinity of these 11 samples probably reflects an abundance of clay (illite) or K-feldspar.

6.2.2. Igneous affinity based on major elements

Considering that most of the samples have an igneous signature, we applied the classical diagrams to classify and distinguish the chemical characteristics of the igneous rock sources (e.g., Cox et al., 1979; Kuno, 1968), as has been applied in previous studies (e.g., Pinto et al., 2004).

In the samples of this study with an igneous affinity, most of those from the lower unit fall within the calc-alkaline rocks domain between the andesitic and rhyolitic fields (Fig. 12). In addition, this progression has a temporal order, with the older samples (LP-01 and IQ-03) falling in an intermediate domain and the younger samples falling close to the rhyodacitic domain. Sample LP-02 is an exception to this trend, since it lies within the alkaline igneous domain. In the middle unit, all of the samples have igneous compositions with dacitic affinities (Fig. 12). In the upper unit, samples with igneous affinities have two distinct compositions, between the dacitic and rhyodacitic fields (MA-01, OM-01, OM-02 and VH-01), whereas other samples (MA-06 and MA-07) show a basaltic signature, rich in Al and poor in K (Fig. 12) (see below).

On the basis of the classic volcanic rock classification diagram (Fig. 13a) (Le Maitre et al., 1989), all of the samples have subalkaline compositions, mainly distributed between the andesitic and rhyodacitic fields. The andesitic compositions assigned to samples LP-01, LP-02 and IQ-03 are in agreement with the results from the discrimination diagram provided by de La Roche (1968) (Figs. 12 and 13a). The AFM diagram (Kuno, 1968) classifies all of the samples as calc-alkaline, although sample AL-16 falls on the border with the tholeiitic field (Fig. 13b). Most of the samples are high in K, the exceptions being MA-06 (low amounts of K) and MA-07, LP-01, LP-02 and BO-01 (medium amounts of K), which is consistent with the basic affinity for these samples inferred from the discrimination diagrams produced by de La Roche (1968) (Fig. 12).

In comparison with the chemical characteristics shown by the studied sedimentary rocks, the two igneous samples from the succession represent end-member characters. The sample from the volcanic breccia (JM-1) was classified as an alkaline rock (Figs. 12 and 13a). Sample RD-1 was classified as granite next to the alkaline domain with 73.52% SiO_2 (Figs. 12 and 13a, and Table 3).

6.2.3. Trace elements signatures of the igneous sources

Major advances in the development of discrimination tectonomagmatic diagrams have been achieved with immobile trace element analysis such as Ti, Zr, Y, Nb and P (e.g., Winchester and Floyd, 1977; Yang et al., 2011). Their behavior is relatively immobile compared to aqueous fluids and they are stable under conditions of hydrothermal alteration up to intermediate metamorphic grades (e.g., Pearce and Cann, 1973). Furthermore, Pinto et al. (2004) proposed the careful use of the igneous discriminant diagram given by Winchester and Floyd (1977) for detrital sedimentary rocks $\log(Zr/TiO_2)$ vs. $\log(Nb/Y)$ (Fig. 14a). Winchester and Floyd (1977) showed that the elements Ti, Zr, Y, Nb, Ce, Ga and Sc can demonstrate the chemical trend of igneous rocks without problems, regardless of

Table 3
Geochemical analyses of whole-rock of samples from the Chinches Formation.

Element	Detection limit	LP-02	LP-01	JM-1	IQ-02	IQ-01	IQ-03	AL-01	AL-02	AL-03	AL-04	AL-05	AL-06	AL-07	AL-08	AL-09	AL-10	AL-11	AL-12	AL-13
SiO_2	0.01	57.56	56.38	56.29	52.4	51.79	56.66	58.85	59.74	57.68	60.76	57.22	57.53	59.77	58.56	59.82	54.64	50.9	55.7	58.18
Al_2O_3	0.01	16.79	14.87	16.82	12.59	11.55	15.05	13.94	13.12	13.23	13.27	12.82	13.33	12.74	12.37	12.54	12.52	13.17	12.83	11.89
Fe_2O_3t	0.01	4.64	6.06	6.17	5.31	3.88	5.19	4.59	3.57	4.41	4.57	3.52	4.36	3.89	4.63	4.24	3.6	4.85	4.41	3.45
MnO	0.001	0.09	0.106	0.179	0.177	0.22	0.093	0.154	0.173	0.155	0.125	0.19	0.176	0.186	0.183	0.143	0.2	0.201	0.127	0.15
MgO	0.01	1.8	3.54	1.57	1.9	1.34	3.3	2.09	1.18	1.36	2.39	1.3	2.17	1.13	1.97	1.78	1.89	1.72	2	1.6
CaO	0.01	5.18	5.05	5.51	10.94	13.27	5.39	6.39	8.02	7.94	5.43	8.85	8.02	8.18	8.12	7.73	10.56	11.88	8.74	8.67
Na_2O	0.01	4.45	2.36	4.85	2.25	2.07	2.97	2.8	2.63	2.6	2.54	1.86	2.39	2.7	2.33	2.45	2.67	2.69	2.65	2.4
K_2O	0.01	1.64	1.4	3.22	2.24	2.52	2.18	2.61	2.88	2.75	2.63	3.03	2.73	3.05	2.62	3.09	2.51	2.23	2.12	2.61
TiO_2	0.001	0.541	0.907	0.7	0.841	0.682	0.72	0.641	0.509	0.661	0.67	0.517	0.595	0.531	0.725	0.618	0.527	0.683	0.639	0.489
P_2O_5	0.01	0.16	0.18	0.29	0.13	0.16	0.19	0.15	0.14	0.14	0.12	0.13	0.13	0.16	0.15	0.15	0.13	0.22	0.16	0.12
LOI		6.89	9.38	2.99	11.01	11.93	8.13	7.19	7.76	8.56	6.72	10.93	9.15	7.71	8.42	7.66	10.06	10.72	9.04	9.3
Total	0.01	99.74	100.2	98.58	99.79	99.41	99.87	99.4	99.72	99.48	99.23	100.4	100.6	100.1	100.1	100.2	99.33	99.26	98.42	98.88
Sc	1	10	14	8	11	11	12	10	9	10	10	9	10	9	9	9	9	11	9	7
Be	1	1	1	1	2	1	1	2	2	2	2	2	2	1	1	2	1	1	1	2
V	5	101	161	110	98	119	112	87	69	99	86	104	82	91	96	85	78	122	95	64
Ba	3	565	298	754	566	957	499	745	962	472	659	977	579	499	690	776	583	857	1121	1378
Sr	2	851	358	434	408	304	422	327	384	288	261	241	266	258	280	236	287	386	312	276
Y	2	15	20	20	27	24	22	25	22	25	25	27	27	24	27	27	25	23	24	26
Zr	4	88	172	176	222	155	170	187	181	194	202	204	200	197	244	197	176	170	191	200
Cr	20	<20	20	<20	80	40	40	40	<20	40	40	<20	40	<20	60	40	30	30	30	20
Co	1	10	15	13	13	9	15	10	6	11	11	7	11	8	12	10	9	11	11	8
Ni	20	<20	<20	<20	40	20	20	<20	<20	20	20	<20	<20	<20	30	<20	<20	<20	<20	<20
Cu	10	350	210	20	20	30	30	20	20	30	20	20	20	20	20	20	30	30	30	30
Zn	30	60	90	90	90	90	100	90	60	90	90	70	100	70	90	80	80	90	80	70
Ga	1	17	17	19	15	14	18	17	15	16	16	15	17	15	15	15	16	15	15	14
Ge	1	2	2	2	2	1	2	2	2	2	2	1	2	2	2	1	1	1	1	1
As	5	6	<5	<5	9	<5	<5	8	6	6	7	12	11	7	10	11	8	8	5	5
Rb	2	39	43	85	77	72	68	81	83	87	85	88	91	84	80	93	85	63	64	81
Nb	1	5	7	11	11	11	11	10	10	12	10	13	12	10	11	12	10	10	10	13
Mo	2	<2	<2	<2	<2	<2	<2	<2	<2	<2	<2	<2	<2	<2	<2	<2	<2	<2	<2	<2
Ag	0.5	<0.5	0.7	0.8	0.6	<0.5	0.5	0.6	0.5	0.6	0.6	0.6	0.5	0.7	0.8	0.6	0,5	0.5	0.6	0.6
In	0.2	<0.2	<0.2	<0.2	<0.2	<0.2	<0.2	<0.2	<0.2	<0.2	<0.2	<0.2	<0.2	<0.2	<0.2	<0.2	<0.2	<0.2	<0.2	<0.2
Sn	1	<1	2	1	2	2	2	2	2	2	2	2	2	2	2	2	2	2	2	2
Sb	0.5	<0.5	<0.5	<0.5	<0.5	<0.5	<0.5	<0.5	<0.5	<0.5	<0.5	<0.5	<0.5	<0.5	<0.5	<0.5	<0.5	<0.5	<0.5	<0.5
Cs	0.5	1.8	2	1.6	7.4	4.3	5.5	4.9	4.7	5.4	5.7	7	7.4	3.7	4.7	5.8	5.3	3.8	3.8	5.1
La	0.1	13.9	22.9	26.4	31.6	30.7	31.4	32.6	32.2	32.3	31	32.3	32.7	29.3	31.5	31.3	39.1	31.2	28.9	31.9
Ce	0.1	26.5	45.6	51.9	62.4	60.3	61.4	64.2	63	63.3	60.8	63	69.5	59.1	64.5	61.8	79.9	64	58.2	64.9
Pr	0.05	3.7	6.15	6.44	7.05	6.8	6.87	7.14	6.87	7.09	6.73	7	7.91	6.67	7.2	7.07	8.76	7	6.58	7.25
Nd	0.1	14.9	24.5	25.1	28.1	27.3	27.8	27.9	26.3	28.2	26.1	26.8	30	25.8	28	26.6	34	27.2	25.8	27.9
Sm	0.1	3.3	5.1	4.9	5.8	5.6	5.9	5.7	5.3	5.9	5.4	5.6	6.2	5.3	5.9	5.8	6.7	5.5	5.3	5.7
Eu	0.05	1.01	1.33	1.36	1.26	1.29	1.39	1.27	1.11	1.22	1.14	1.06	1.18	1.14	1.2	1.11	1.16	1.28	1.21	1.09
Gd	0.1	2.8	4.2	4.3	5	4.7	4.8	4.7	4.4	4.9	4.6	4.6	4.9	4.4	5.1	4.8	5.1	4.7	4.4	4.8
Tb	0.1	0.5	0.7	0.7	0.8	0.8	0.8	0.7	0.7	0.8	0.8	0.7	0.8	0.7	0.8	0.8	0.8	0.7	0.7	0.8
Dy	0.1	2.8	4.2	4	4.5	4.2	4.2	4.3	4.1	4.5	4.4	4.3	4.5	4.1	4.5	4.6	4.4	4.1	4.3	4.3
Ho	0.1	0.5	0.8	0.8	0.9	0.8	0.8	0.8	0.8	0.9	0.9	0.9	0.9	0.8	0.9	0.9	0.9	0.8	0.9	0.9
Er	0.1	1.5	2.1	2.3	2.6	2.4	2.4	2.5	2.4	2.6	2.5	2.6	2.5	2.6	2.6	2.7	2.5	2.4	2.5	2.6
Tm	0.05	0.23	0.33	0.34	0.39	0.37	0.37	0.37	0.36	0.4	0.38	0.4	0.39	0.4	0.4	0.43	0.38	0.35	0.38	0.4
Yb	0.1	1.6	2.2	2.4	2.6	2.5	2.4	2.5	2.4	2.7	2.6	2.9	2.7	2.7	2.7	2.9	2.6	2.4	2.6	2.8
Lu	0.04	0.25	0.35	0.38	0.42	0.41	0.39	0.43	0.4	0.44	0.43	0.48	0.44	0.44	0.45	0.46	0.42	0.39	0.41	0.45
Hf	0.2	2.6	4.7	4.8	5.5	3.9	4.3	4.6	4.5	5	4.9	5.1	5	5	6.1	5	4.4	4.4	4.9	5.1
Ta	0.1	0.3	0.5	0.7	0.9	0.8	0.9	0.9	0.8	0.9	0.9	0.9	0.9	0.8	0.9	0.8	0.8	0.8	0.8	0.9
W	1	3	3	3	<1	<1	<1	3	<1	3	<1	<1	<1	<1	<1	<1	<1	<1	<1	<1
Tl	0.1	0.3	0.3	0.5	0.4	0.3	0.4	0.4	0.4	0.4	0.4	0.4	0.4	0.4	0.4	0.5	0.4	0.3	0.3	0.4
Pb	5	8	12	8	21	18	23	23	21	25	23	21	24	18	21	22	19	21	18	16
Bi	0.4	< 04	<0.4	<0.4	<0.4	<0.4	<0.4	<0.4	<0.4	<0.4	<0.4	<0.4	<0.4	<0.4	<0.4	<0.4	<0.4	<0.4	<0.4	<0.4
Th	0.1	3.2	5.8	6.6	7.4	6.2	8.1	7.8	8	8.3	7.9	8.4	8.2	7.6	7.6	7.6	7.7	6.7	6.7	8
U	0.1	1.1	2.3	1.8	2	1.7	1.9	2.2	2	2.3	2.2	2.4	2.1	1.9	2.1	2	2.5	2	2.1	2.1
Eu/Eu^*	–	1.02	0.88	0.91	0.72	0.77	0.80	0.75	0.70	0.69	0.70	0.64	0.65	0.72	0.67	0.64	0.61	0.77	0.77	0.64
La_N/Yb_N	–	6.23	7.47	7.89	8.72	8.81	9.38	9.35	9.62	8.58	8.55	7.99	8.69	7.78	8.37	7.74	10.79	9.32	7.97	8.17

Element	Detection limit	AL-14	AL-15	AL-16	BO-01	PA-02	PA-03	PA-01	OM-02	OM-01	VH-01	MA-01	MA-02	MA-03	MA-04	MA-05	MA-06	MA-07	MA-10	RD-1
SiO_2	0.01	67.47	54.61	53.71	63.9	58.08	65.65	60.07	55.07	65.5	65.65	55	61.08	59.4	54.77	44.79	51.75	53.26	54.8	73.52
Al_2O_3	0.01	11.6	9.36	11.1	14.3	12.56	10.38	11.82	11.99	14.3	13.46	14.7	10.03	12.1	10.68	8.4	19.49	18.45	10.99	13.63
Fe_2O_3t	0.01	3.33	3.07	4.92	5.05	3.37	3.82	4.16	4.49	4.1	3.84	4.92	2.6	3.77	3.48	2.62	3.81	2.55	3.6	1.6
MnO	0.001	0.084	0.228	0.219	0.069	0.125	0.092	0.11	0.115	0.08	0.074	0.115	0.064	0.09	0.09	0.072	0.074	0.069	0.08	0.068
MgO	0.01	1.17	0.79	1.16	2.45	1.73	0.89	1.35	1.7	1.58	1.21	1.41	0.7	1.26	1.04	0.77	2.37	1.75	1.19	0.32
CaO	0.01	4.53	13.27	12.76	3.09	9.02	6.77	8.55	10.49	3.56	3.62	8.84	10.15	7.3	11.47	19.09	6.93	7.87	9.59	0.93
Na_2O	0.01	2.65	2.19	2.33	3.45	2.25	2	2.21	2.12	2.86	2.61	3.27	1.37	1.61	1.32	0.96	3.4	3.35	0.79	4.27
K_2O	0.01	3.14	2.27	2.51	2.15	2.86	3.19	3.16	2.12	2.69	2.76	2.12	3.75	3.21	3.03	2.6	0.44	1.02	2.71	4.48
TiO_2	0.001	0.469	0.484	0.721	0.64	0.605	0.568	0.636	0.683	0.562	0.53	0.645	0.364	0.555	0.52	0.378	0.536	0.357	0.529	0.222
P_2O_5	0.01	0.11	0.1	0.17	0.16	0.15	0.11	0.15	0.15	0.13	0.13	0.17	0.1	0.13	0.11	0.18	0.2	0.12	0.12	0.07
LOI		4.77	12.24	11.19	3.64	9.59	6.13	7.82	9.58	4.91	4.94	8.77	9.94	10.07	13.51	18.59	10.16	10.4	14.18	0.84
Total	0.01	99.32	98.62	100.8	98.91	100.3	99.59	100	98.52	100.3	98.83	99.95	100.2	99.51	100	98.45	99.17	99.21	98.56	99.94
Sc	1	7	8	11	12	10	8	9	10	8	8	11	7	9	8	7	7	6	9	4
Be	1	1	<1	1	2	1	1	1	1	2	2	2	2	2	2	1	1	1	2	3
V	5	64	62	115	96	91	80	82	95	76	72	99	50	63	61	47	74	44	63	<5
Ba	3	648	1006	990	455	776	575	728	767	568	700	606	1165	543	506	346	429	373	737	932
Sr	2	215	226	263	298	265	272	350	534	401	430	658	1159	296	220	190	961	836	344	63
Y	2	25	23	26	18	25	25	26	22	18	21	18	27	27	26	24	8	10	23	43
Zr	4	190	192	188	128	196	192	198	228	150	155	149	179	223	219	147	126	104	237	227
Cr	20	30	30	40	<20	30	40	40	50	20	20	<20	<20	20	20	<20	<20	<20	20	<20
Co	1	7	5	8	13	9	7	10	11	9	8	10	5	8	7	5	9	5	5	<1
Ni	20	<20	<20	<20	<20	<20	<20	<20	<20	<20	<20	<20	<20	<20	<20	<20	<20	<20	<20	<20
Cu	10	30	20	20	20	20	20	20	30	20	20	20	10	20	10	10	20	20	20	<10
Zn	30	60	50	80	100	90	60	60	70	60	60	80	60	80	70	50	70	60	80	60
Ga	1	13	11	13	17	15	13	14	14	16	15	17	12	15	13	10	21	20	13	16
Ge	1	2	1	1	1	1	2	2	1	2	1	1	2	2	1	1	<1	1	1	2
As	5	5	9	8	6	20	12	10	9	6	7	6	10	11	11	8	<5	<5	11	<5
Rb	2	95	70	70	79	83	105	96	70	96	97	71	117	105	93	78	8	32	87	164
Nb	1	10	9	10	7	11	10	12	11	8	9	8	11	10	12	7	5	4	9	14
Mo	2	<2	<2	<2	<2	<2	<2	<2	<2	<2	<2	<2	<2	<2	<2	<2	<2	<2	<2	<2
Ag	0.5	0.6	<0.5	0.6	0.5	0.6	0.8	0.8	1	0.5	0.6	<0.5	<0.5	0.7	0.6	<0.5	<0.5	<0.5	0.6	0.6
In	0.2	<0.2	<0.2	<0.2	<0.2	<0.2	<0.2	<0.2	<0.2	<0.2	<0.2	<0.2	<0.2	<0.2	<0.2	<0.2	<0.2	<0.2	<0.2	<0.2
Sn	1	2	1	2	2	2	2	2	2	2	2	2	2	2	2	1	<1	1	2	3
Sb	0.5	0.6	<0.5	0.5	0.7	0.6	1.6	1.3	1.1	0.9	0.9	<0.5	0.7	0.7	0.6	<0.5	<0.5	<0.5	0.7	<0.5
Cs	0.5	4.3	6	3.9	2.9	5.5	6.5	6.4	7.4	4.1	4.7	3.2	8.8	11.6	8.7	6.1	1.2	6.1	8.6	1.7
La	0.1	28.8	25.9	28.3	26.6	31.4	23.2	26.3	25.5	22.6	27.4	25.8	26.2	32.8	29.8	24.9	14.7	19.5	26.8	49.6
Ce	0.1	56.7	53.1	54.4	53.3	60.9	45.3	50.9	47.7	44.8	52.9	51.2	49.2	60.4	50.6	43.5	31.5	37.4	52.8	98.1
Pr	0.05	6.35	6.29	6.24	6.69	6.84	5.81	6.59	6.24	5.5	6.69	5.66	5.71	6.95	6.37	5.41	3.39	4.06	5.73	9.85
Nd	0.1	24.4	24.9	24.9	25.3	27.1	23	25.3	24.1	20.9	25.1	22.6	22.4	27.6	25.2	21.2	14.1	16.2	22.4	34.8
Sm	0.1	5.2	5.2	5.2	5.2	5.4	4.7	5.4	5.2	4.2	5	4.6	4.7	5.8	5.2	4,8	3	3	4.7	7.1
Eu	0.05	1	1.01	1.16	1.11	1.16	0.98	1.14	1.16	0.97	1.07	1.08	0.85	1.09	0.97	0,98	0.95	0.97	0.96	0.87
Gd	0.1	4.4	4.4	4.8	4.1	4.6	4.1	4.8	4.5	3.6	4.2	3.8	4.3	5	4.4	4,1	2.1	2.6	4.1	6.1
Tb	0.1	0.7	0.7	0.8	0.7	0.8	0.7	0.8	0.7	0.6	0.7	0.6	0.8	0.8	0.7	0,7	0.3	0.4	0.7	1.1
Dy	0.1	4.3	3.9	4.3	3.7	4.4	4.6	5	4.4	3.4	4.2	3.5	4.6	4.5	4.4	4,1	1.6	2.1	3.9	6.8
Ho	0.1	0.9	0.8	0.9	0.7	0.9	0.9	1	0.9	0.7	0.8	0.7	0.9	0.9	0.9	0,8	0.3	0.4	0.8	1.4
Er	0.1	2.6	2.3	2.6	2	2.6	2.7	2.8	2.4	1.9	2.3	2	2.8	2.6	2.6	2,4	0.8	1.1	2.3	4.4
Tm	0.05	0.41	0.36	0.39	0.29	0.38	0.43	0.42	0.38	0.29	0.36	0.31	0.43	0.42	0.4	0,37	0.12	0.17	0.35	0.7
Yb	0.1	2.8	2.4	2.6	1.9	2.6	2.8	2.8	2.5	1.9	2.4	2.1	3	3	2.8	2,6	0.8	1.1	2.5	5
Lu	0.04	0.47	0.4	0.42	0.3	0.43	0.46	0.44	0.4	0.32	0.39	0.33	0.48	0.48	0.46	0,44	0.13	0.19	0.43	0.85
Hf	0.2	4.9	4.8	4.7	3.6	4.8	5.1	5.5	6.2	4.1	4.5	3.9	4.7	5.4	5.3	3,7	3.2	2.7	5.8	6.8
Ta	0.1	0.8	0.6	0.7	0.6	0.8	0.8	0.9	0.7	0.7	0.7	0.6	0.9	0.8	0.8	0,6	0.3	0.3	0.8	1.2
W	1	<1	3	<1	4	<1	4	4	4	4	4	<1	<1	1	<1	<1	<1	<1	<1	<1
Tl	0.1	0.5	0.3	0.3	0.5	0.4	0.7	0.6	0.5	0.6	0.6	0.3	0.5	0.5	0.5	0,4	<0.1	0.2	0.4	0.7
Pb	5	16	14	17	14	18	15	14	16	15	16	15	15	22	18	15	12	15	21	24
Bi	0.4	<0.4	<0.4	<0.4	<0.4	<0.4	<0.4	<0.4	<0.4	<0.4	<0.4	<0.4	<0.4	<0.4	<0.4	<0.4	<0.4	<0.4	<0.4	<0.4
Th	0.1	7.8	6	6.1	7.5	7.2	7.6	7.6	6.7	8.4	8.5	7.4	8.5	8.9	8.3	6,8	3.5	4.1	7.7	21.3
U	0.1	2	1.7	1.6	1.8	2.5	1.9	2.1	2.1	2.1	2.2	1.9	2	2.5	2.2	1,8	0.7	1	2.1	2.7
Eu/Eu*	–	0.64	0.65	0.71	0.73	0.71	0.68	0.68	0.73	0.76	0.71	0.79	0.58	0.62	0.62	0.68	1.16	1.06	0.67	0.40
La_N/Yb_N	–	7.38	7.74	7.81	10.04	8.66	5.94	6.74	7.32	8.53	8.19	8.81	6.26	7.84	7.63	6.87	13.18	12.72	7.69	7.12

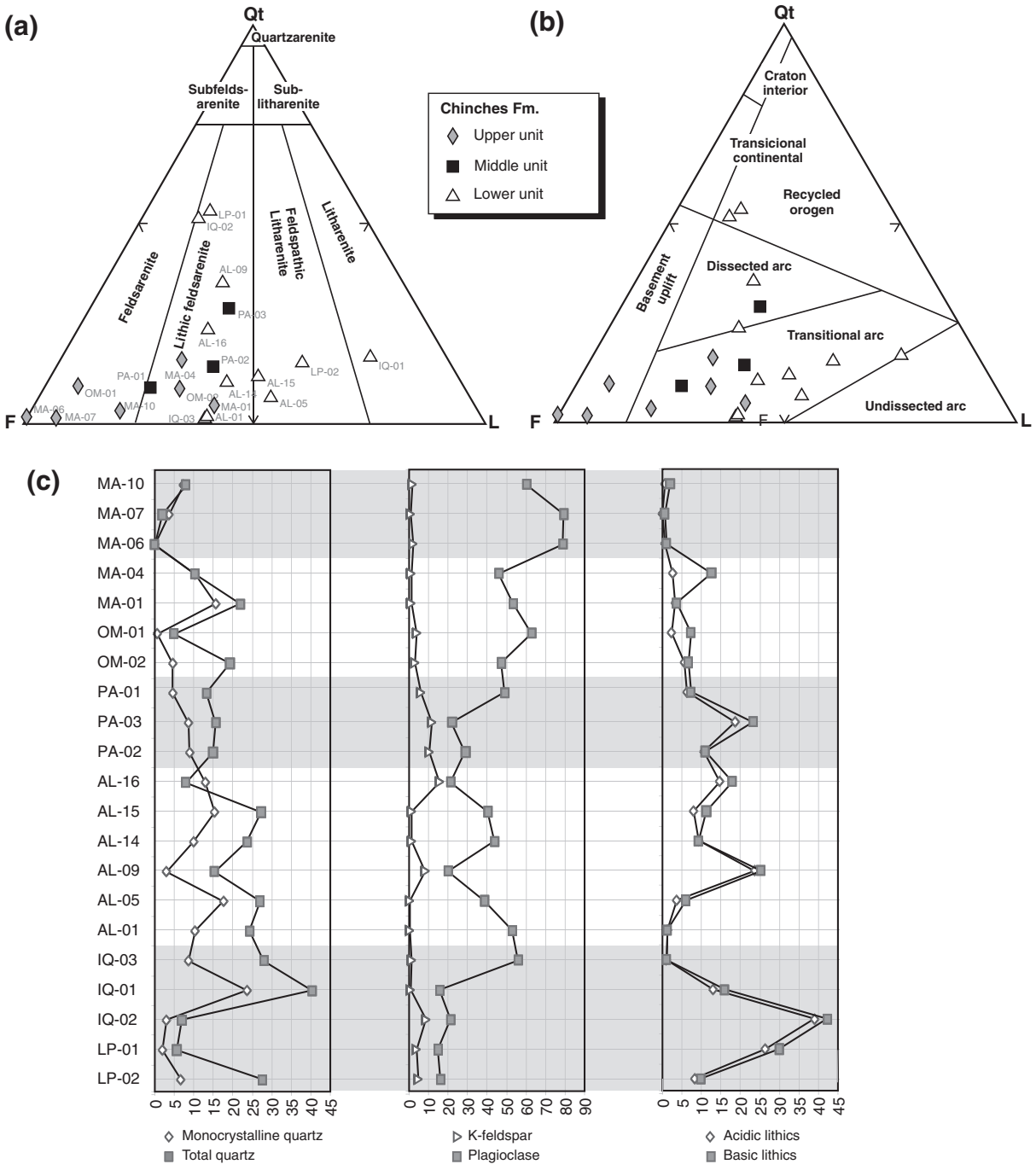

Fig. 5. (a) Qt–F–L, sandstone classification diagram according to Folk et al. (1970). (b) Qt–F–L, diagram with tectonic fields of Dickinson et al. (1983). Qt: total quartz (mono- and polycrystalline grains), F: feldspar (plagioclase and K-feldspar), L: lithic rock fragments. The location of samples relative to the triangle is the same as in 'a'.(c) Variation diagrams of mineral and lithic percentages in the studied sandstones (based on Table 2).

major elements such as the SiO_2 index, differentiating between the types of rocks as well as distinguishing the magmatic series. The authors proposed that the discriminatory diagram can be used even in rocks that have undergone metamorphism or have been extensively altered. Therefore, in this study we used the $\log(Zr/TiO_2)$ vs. $\log(Nb/Y)$ diagram (Fig. 14a) to confirm and provide details of the geochemistry of the igneous source rocks that supplied material to the Chinches Formation.

All of our samples fall in the sub-alkaline field (Fig. 14a). The general trend is similar to that in Fig. 10 and indicates that samples from the base of the lower unit of the succession are clearly andesitic-dominated (Fig. 14d). Those in the rest of the lower unit, all of those in the middle unit, and those at the base of the upper unit (Fig. 14b and c) fall within the dacitic domain. Finally, the samples from the top of the upper unit fall within the rhyodacitic domain. The geochemical trend shown by the trace and major elements is similar (Figs. 12 and 14a). Based on this, the $\log(Zr/TiO_2)$ shows a stratigraphic progression from least to most differentiated igneous rock sources.

The plot of La/Th vs. Hf also provides useful bulk discrimination between different arc compositions and sources (Bathia and Taylor, 1981; Taylor and McLennan, 1985; Floyd and Leveridge, 1987; Kutterolf et al.,

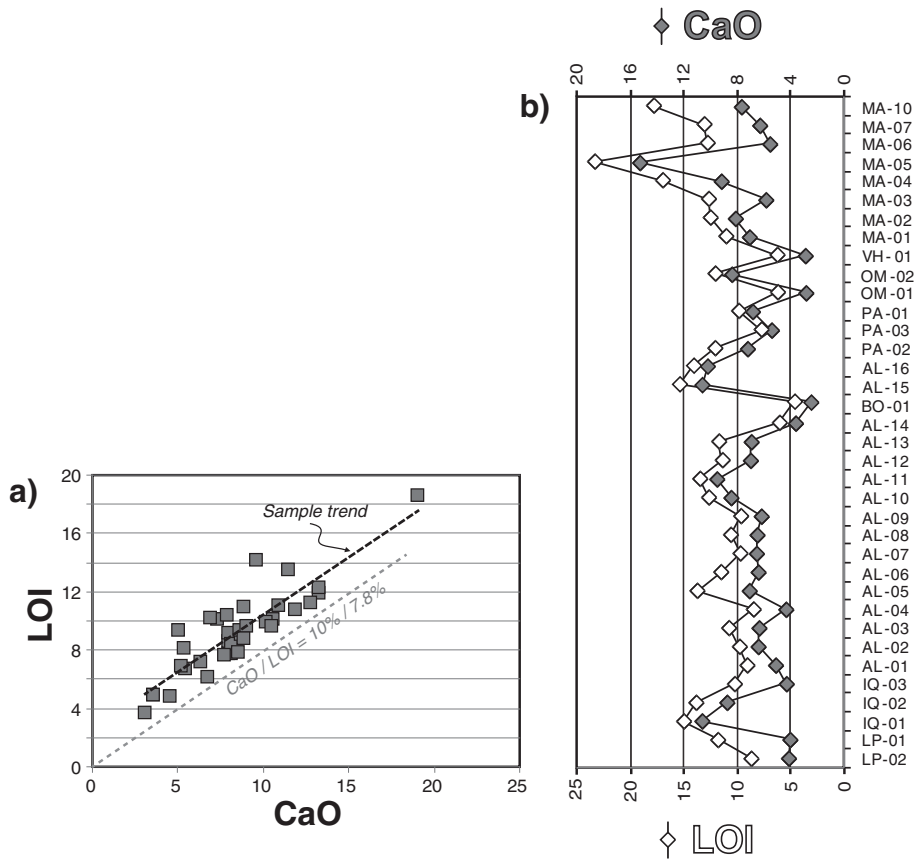

Fig. 6. Graphs showing the relationship between CaO and LOI in the studied sedimentary rocks and the presence of calcite: a) LOI vs. CaO wt.% are represented on a bi-dimensional diagram, showing the almost linear relationship; b) CaO and LOI wt.% are represented on a spider diagram after their stratigraphic position, showing a similar pattern.

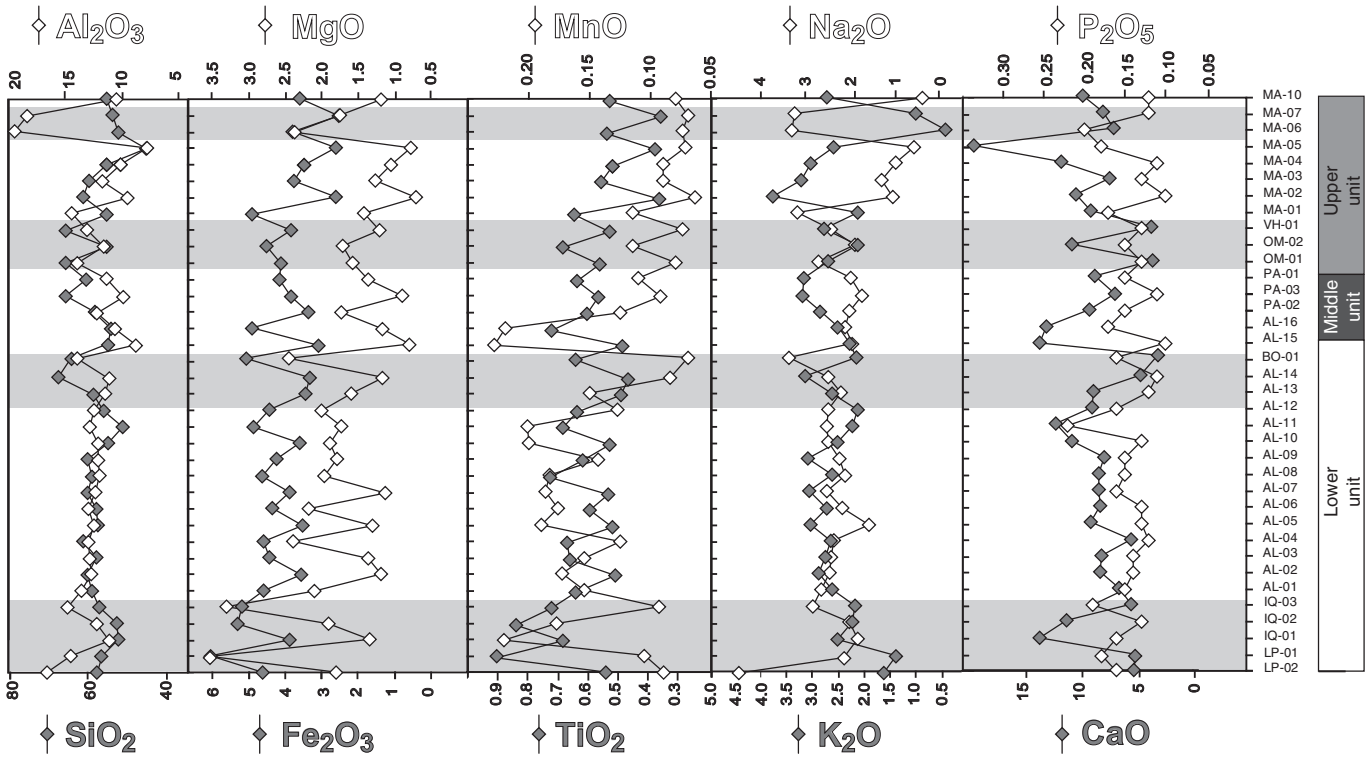

Fig. 7. Chemostratigraphy of the major paired elements according to their affinity with the sedimentary samples of this study (elements are given in wt.%). Gray bars are shown to visualize the correlations between the elements. The stratigraphic units defined in this study are shown.

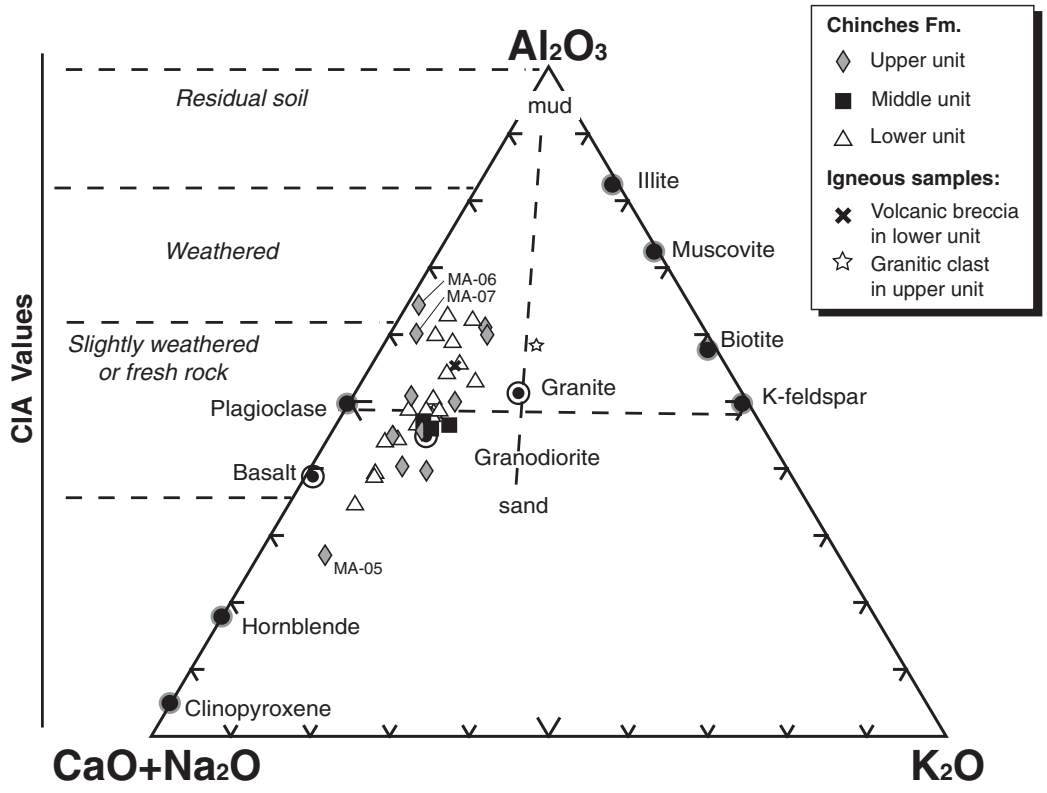

Fig. 8. (CaO + Na_2O), K_2O and Al_2O_3 and CIA values (Chemical Index of Alteration) diagram to analyze the chemical alteration of the sedimentary rocks proposed by Fedo et al. (1995) and Nesbitt and Young (1982, 1984) and applied to the sedimentary rocks of this study. Elements are given in wt.%. CIA is defined as Al_2O_3 / (Al_2O_3 + CaO* + Na_2O + K_2O) × 100 (molar contents, where CaO* is the CaO content in the silicate fraction for the sample).

2008; Yang et al., 2011). Given the particular character of samples MA-06 and MA-07, we did not consider them for the general analysis (Fig. 15). In general, the studied sedimentary rocks fall mainly within the acidic arc source, having La/Th ratios of 2.7–5.1 (3.9 on average) and Hf contents of about 2.6–6.2 (4.7 on average) (Table 3). The lower unit of the Chinches Formation has higher values of La/Th (3.7–5.1, 4.2 on average) and is well discriminated from the upper unit (2.7–3.8, 3.4 on average) in this graph (Fig. 15). Moreover, the lower unit samples fall in the field of the acidic–basic mixture and the upper unit is more acidic, similar and perhaps more clear than shown by the log(Zr/TiO_2) vs. log(Nb/Y) diagram (Fig. 14).

6.3. Integration of petrography and geochemistry of the Chinches Formation

The petrography and geochemistry of sedimentary rocks studied show two principal source rocks: calcareous and igneous. The calcareous source is evidenced indirectly by the petrography of sandstones,

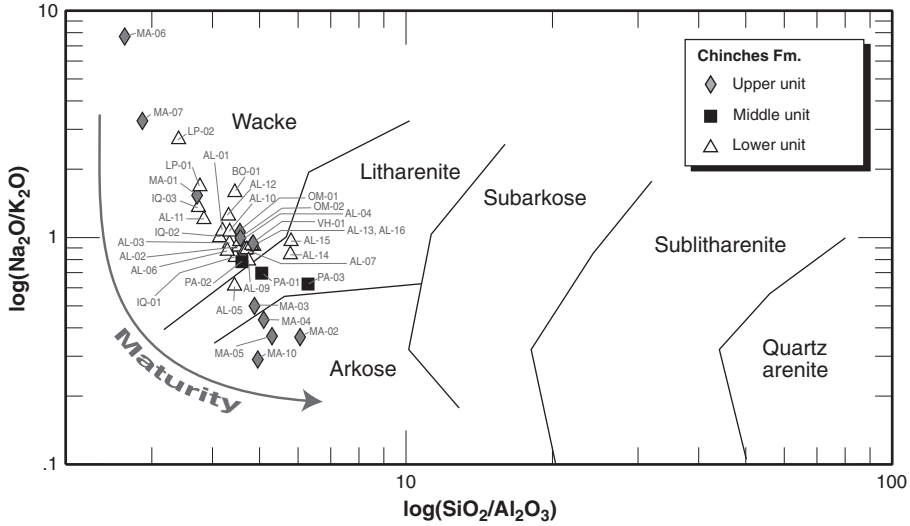

Fig. 9. Classification of the samples on the terrigenous sandstones diagram that use log(Na_2/K_2O) vs. log(SiO_2/Al_2O_3) (elements are given in wt.%) proposed by Pettijohn et al. (1972) and redrawn by Herron (1988).

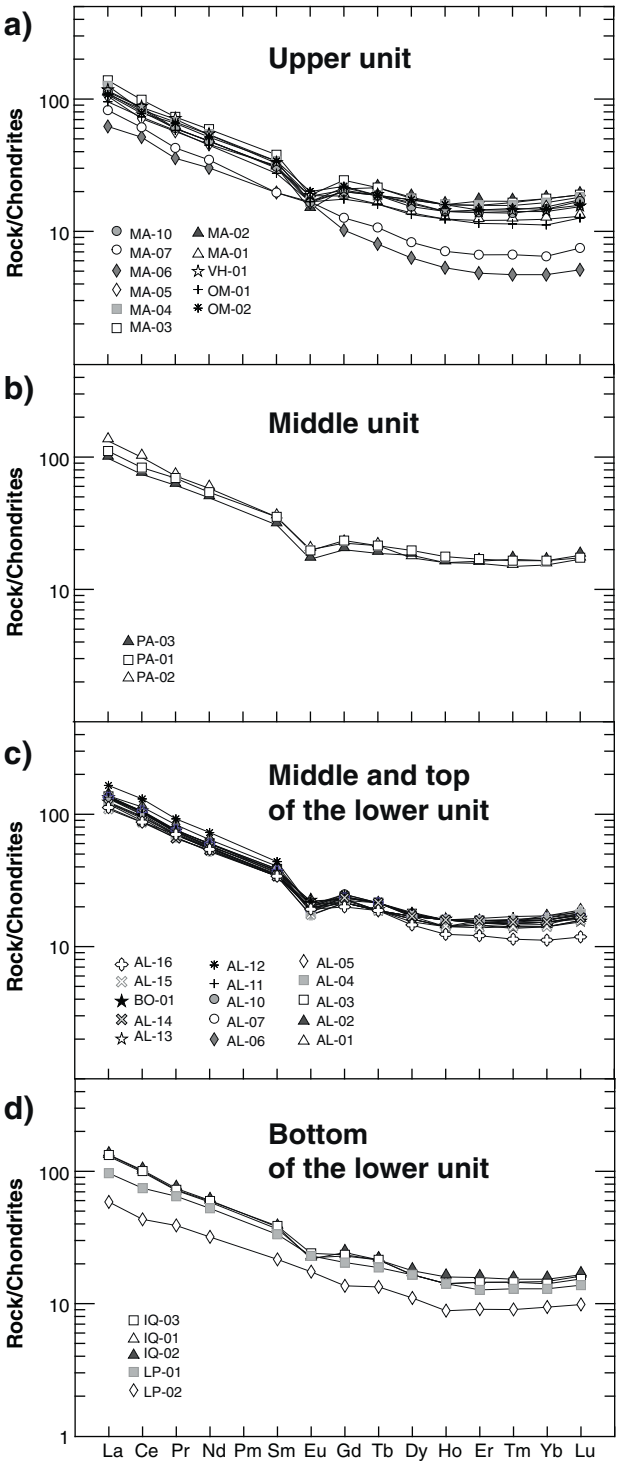

Fig. 10. REE spider diagram normalized to chondrite (after Sun and McDonough, 1989) for the Chinches Formation, according to the stratigraphic units defined in this study.

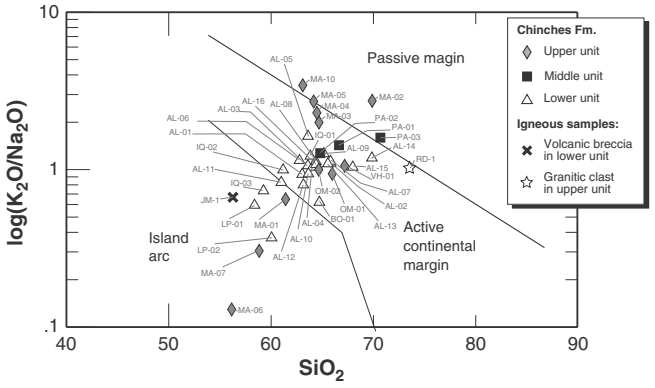

Fig. 11. Log(K_2O / Na_2O) vs. SiO_2 discrimination diagram introduced by Roser and Korsch (1986) applied to the sandstones from the Chinches Formation. Elements are given in wt.%.

which shows abundant calcareous cement in almost all of the samples, with scarce calcareous grains. Moreover, the presence of this calcareous material was recognized in the geochemistry of the samples, with most of them exhibiting >4 wt.% CaO (Fig. 6). Correlated with LOI, this indicates the presence of calcite. Thus, the calcareous signature may probably be related to an input from the Mesozoic units recognized by Pérez (1995, 2001), which includes limestones with tuffaceous material and sandstones (Fig. 3).

The composition of the major elements in the (Al/3-K) vs. (Al/3-Na) diagram (Fig. 12) indicates that the igneous sources were dominant or best preserved in the sedimentary rocks in the lower unit of the succession with respect to the middle and upper units. Moreover, the petrography shows that the igneous sources were significant throughout the global succession. In particular, the petrology and geochemistry show that the upper unit has a slightly high chemical maturity (Figs. 5 and 9) and a high concentration of K-feldspar (Figs. 5, 9 and 12) with respect to the other units. These characteristics reflect a change to a source that was richer in quartz and K-feldspar, such as a granitic source.

The petrography classifies almost all of the samples as lithic feldsarenite, whereas the geochemistry principally classifies them as greywackes due to the limitations of the geochemical database (Herron, 1988; Pettijohn et al., 1972). Moreover, samples show a geochemical trend from greywackes in the lower unit to litharenites in the middle unit and to arkoses in the upper unit (Fig. 9). The correct classification is the petrographic one, but although chemical classification does not coincide exactly with it, both reflect the same progression from sources rich in volcanic lithics towards sources rich in feldspars (Figs. 5 and 9).

There is an overall geochemical trend from intermediate (andesitic) igneous compositions in the sedimentary rocks of the lower unit of the Chinches Formation passing progressively to a more acidic (rhyodacitic) composition in the upper unit, which is evidenced by major and trace elements (Figs. 9, 12, 14 and 15). The sources of these rocks have a sub-alkaline signature (Fig. 12). Moreover, the common geochemical characteristics for the samples from the basal parts of the lower unit to basic/intermediate (island arc) rocks can be associated with a thinned continental crust (Fig. 11), those from the lower and middle units can be associated with an active continental margin composed of acidic rocks (e.g., Taylor et al., 1968) and those from the top with an acidic source. This progression is well related to that reflected in the tectonic discrimination diagram for petrography of sandstones (Fig. 5).

Furthermore, hand specimen observations of samples MA-06 and MA-07 and their petrography (Fig. 5 and Table 2) suggest a volcanic provenance indicated by a high percentage of volcanic ash and volcanic minerals such as plagioclase and hornblende in these samples. Pérez (1995) described these rocks as Plinian fall deposits, however, our petrographic analysis indicates reworking of the material and, therefore, it is sedimentary.

6.4. Geochemistry of the potential source rocks

In the key discrimination diagrams (Figs. 12, 13a, 14 and 15), the geochemical data available for potential source rocks of sediments of the Manantiales Basin were plotted: the Choiyoi Group, Espinacito Granite, Los Pelambres, Abanico, Farellones and Cristo Redentor

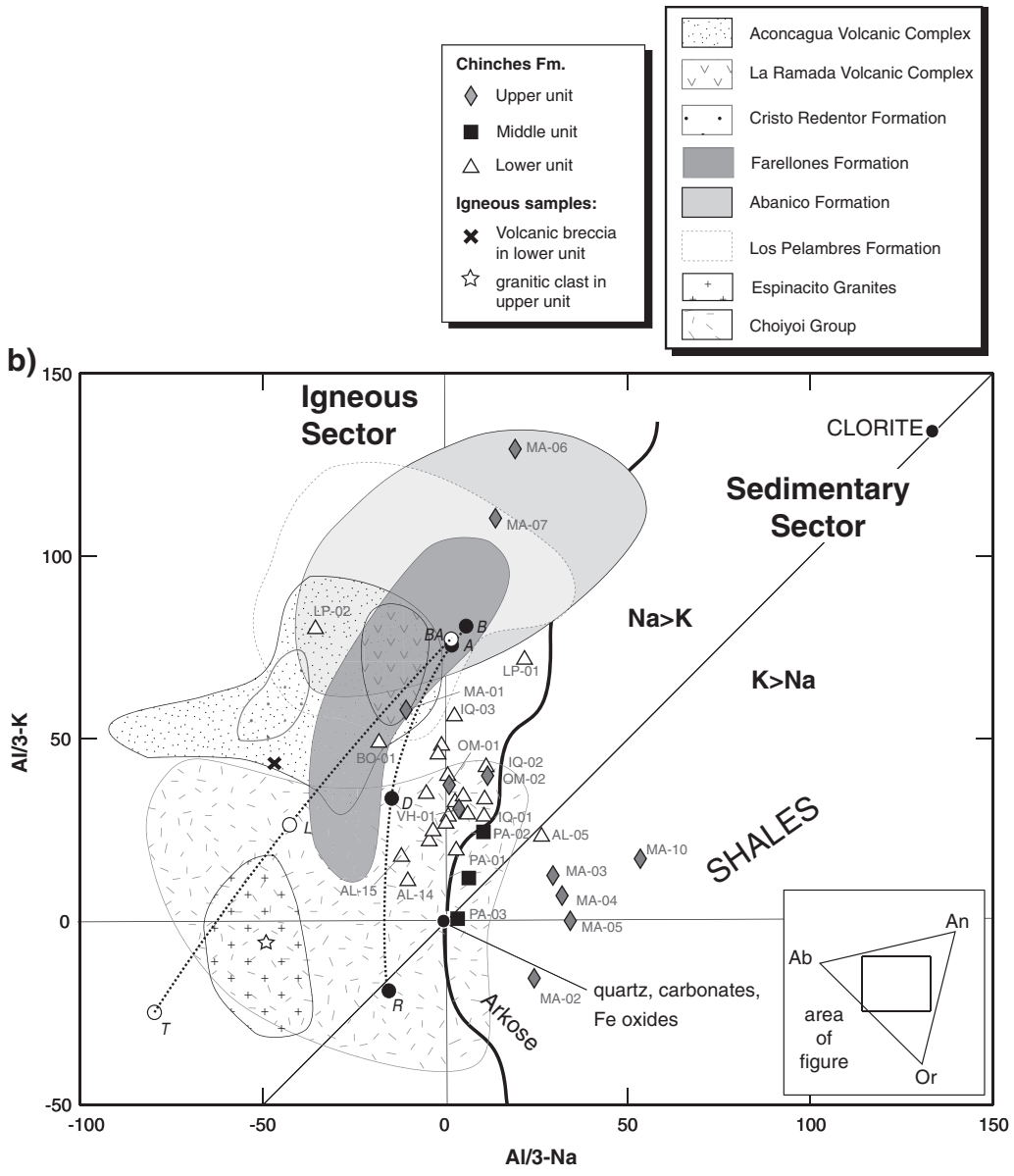

Fig. 12. (Al/3-K) vs. (Al/3-Na) diagram (the elements are given in milliatoms/100 g of rock or mineral; 1 milliatom = 10^{-3} atoms) showing the igneous and sedimentary domains (modified from de La Roche, 1968; Moine, 1974), where the chemistry of the studied sedimentary rocks was plotted. The values were not recalculated because the CaO wt.% had almost no effect on the plot. The location of the end-member minerals is indicated in the triangle at the right (An: Anorthite; Ab: Albite; Or: Orthoclase). The diagram widely disperses the silico-alumina and concentrates the other major fractions near the origin as quartz, carbonates and iron oxides. Clay minerals are distributed within the sector with relatively high values of Al and where Al is predominant over Na. The greywackes and certain immature arkoses remain in the igneous domain. The compositional fields were taken from the database for the potential source rocks given by Vergara et al. (1993), Pérez (1995), Ramos et al. (1996b), Vergara and Nyström (1996), Fuentes (2004), Montecinos (2008), Levi (2010) and Pinto et al. (in preparation). *Calc-alkaline trend*: B, Basalt; A, Andesite; D, Dacite; R, Rhyolite. *Alkaline trend*: BA, Alkaline basalt; L, Latite; T, Traquite. We separate the igneous domain from the sedimentary domain by a thick black line.

(Argentina) Formations and the La Ramada and Aconcagua Volcanic Complexes (Vergara et al., 1993; Pérez, 1995; Ramos et al., 1996b; Vergara and Nyström, 1996; Fuentes, 2004; Montecinos, 2008; Levi, 2010; Pinto et al., in preparation). The Choiyoi Group and Espinacito Granites are the oldest rocks and correspond to the most acidic units, the granites being more limited in their geochemical trends (Figs. 12, 13a, 14 and 15), whereas the Choiyoi Group shows a large spectrum (Figs. 12, 13a and 15) with a tendency towards field magmas with an old sediment component (Fig. 15). The group formed by the Los Pelambres, Abanico, Farellones and Cristo Redentor Formations is similar in geochemistry (Fig. 12), the most basic being the Abanico Formation, followed by the Cristo Redentor Formation which has an acidic–basic mixture, but with an andesitic trend (Figs. 13a and 15). The Los Pelambres and Farellones Formations have an acidic and dacitic (Figs. 12 and 15) tendency. The Farellones Formation is characterized by a broad range of compositions similar to the Choiyoi Group, but more basic (Figs. 12 and 13a). Miocene volcanic complexes are geochemically similar (Fig. 12), although the Aconcagua Volcanic Complex has a more acidic trend (Fig. 15).

6.5. Progression of the igneous sources in the succession

The most remarkable character of the petrography and geochemistry of sedimentary rocks of the Chinches Formation is a progression of diverse igneous rocks from the base to the top of the succession (e.g., Figs. 5, 9, 12, 14). We can suggest the following interpretations for this kind of source rock based on a comparison of its character

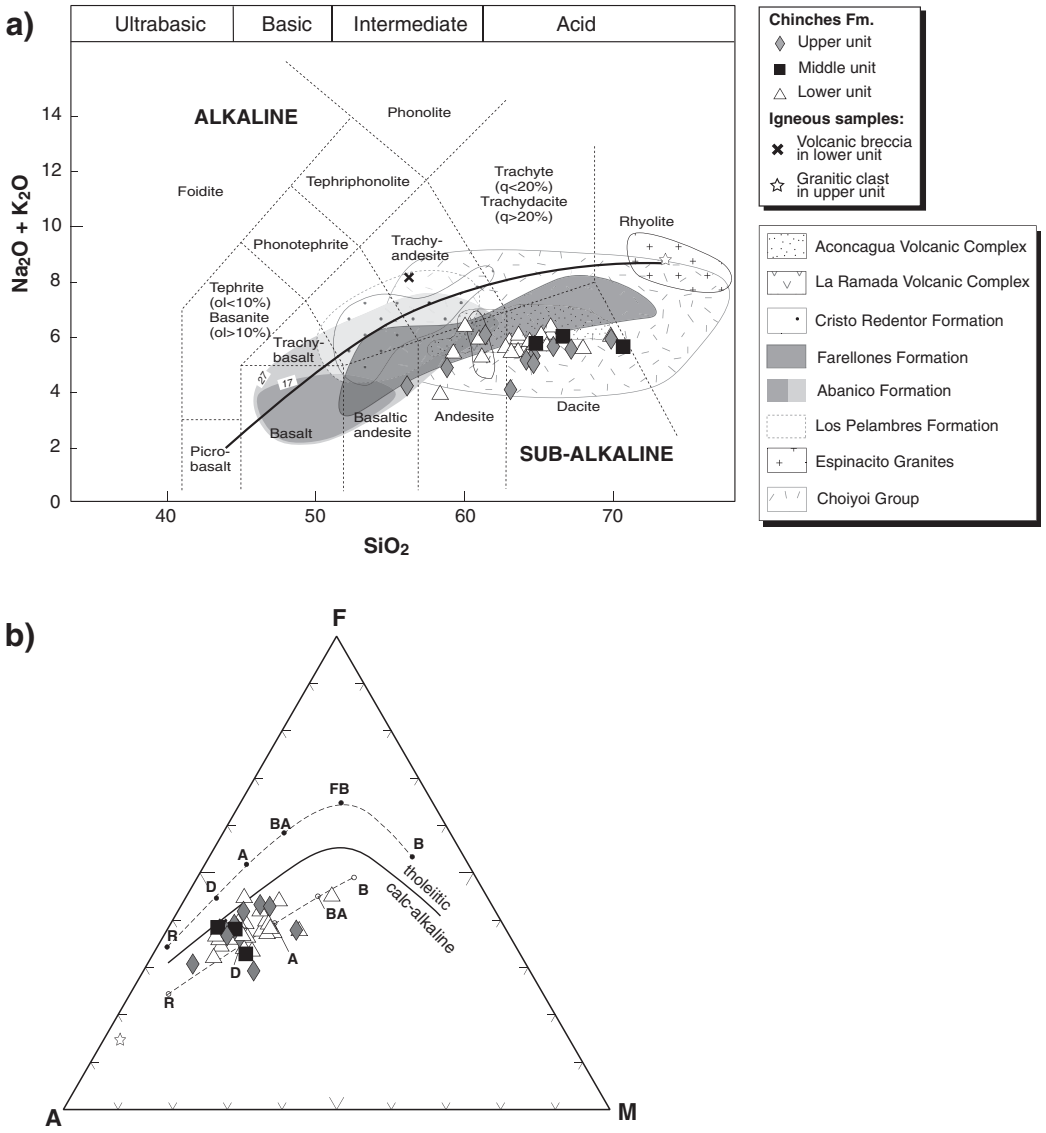

Fig. 13. a) Chemical classification and nomenclature of the volcanic rocks, where the total alkalis ($Na_2O + K_2O$) wt.% vs. silica (SiO_2) wt.% (TAS) is used (after Le Maitre et al., 1989), showing the boundary between the alkaline and subalkaline fields, as well as the division between the ultramafic, mafic, intermediate and acidic character for the igneous rocks. The gray areas for the Abanico Formation indicate the cumulative frequency curves. b) AFM diagram for volcanic rocks showing the boundary between the calc-alkaline and tholeiitic fields (after Kuno, 1968). Abbreviations: R: Rhyolite; D: Dacite; A: Andesite; BA: Andesitic basalt; FB: Ferro-Basalt; B: Basalt; A: $Na_2O + K_2O$; F: FeO + Fe2O3; M: MgO, all in wt.%.

defined by the petrography and geochemistry analyses with that of the potential geological sources.

6.5.1. First stage: volcanic intermediate igneous source

The basal samples of the lower unit of the Chinches Formation (LP-01, LP-02, IQ-01, IQ-02, IQ-03, and Table 1) have a more intermediate (andesitic) character compared to the rest of the succession. This contribution is probably related to the volcanic andesitic breccia located in the lower unit of the Chinches Formation and whose age is assigned to the Early Miocene (Fig. 4) (ca. 20 Ma, Pérez and Ramos, 1996; Pérez, 2001). This breccia, correlated to the Pichireguas Breccia (Pérez, 1995) to the west, has features that can be traced within the sedimentary rocks, and corresponds to a source for the Chinches Formation during its first stage of development. This breccia is coeval with the basal part of the Farellones Formation on the Chilean side (Rivano et al., 1993), and it could have been the source of the Manantiales Basin at this stage. The basal samples of the Chinches Formation present a good affinity with the geochemical field of the Farellones Formation (Figs. 12 and 13a). On the other hand, samples from the lower unit of the Chinches Formation show an affinity to a mixed acidic-basic source similar to the Argentinean Cristo Redentor Formation with a tendency towards the La Ramada Volcanic Complex (Fig. 15). Unfortunately, the database of the Farellones Formation for this diagram is too low (n = 3) to establish a better correlation. Fission-track ages and the magnetostratigraphic analysis of Jordan et al. (1996) allow us to constrain this stage of provenance, represented by basal parts of the Chinches Formation, to the Early Miocene (ca. 19 Ma, Fig. 4).

6.5.2. Second stage: mixing of intermediate and acidic igneous sources

Discriminant plots of the trace elements $\log(Zr/TiO_2)$ vs. $\log(Nb/Y)$ (Fig. 14) and La/Th vs. Hf (Fig. 15) show that the samples have an acidic affinity, mainly dacitic. Samples from the lower and middle units have an affinity with a mixed source of acidic and intermediate rocks (Fig. 15). A potential acidic source corresponds to the rhyolitic and rhyodacitic volcanic rocks of the Choiyoi Group in the Frontal Cordillera (Cordón del Espinacito, Fig. 2b) (Figs. 12–15). The petrology of sedimentary clasts registers a high percentage of rhyolitic fragments (Fig. 16) (Pérez, 1995, 2001) and a higher percentage of

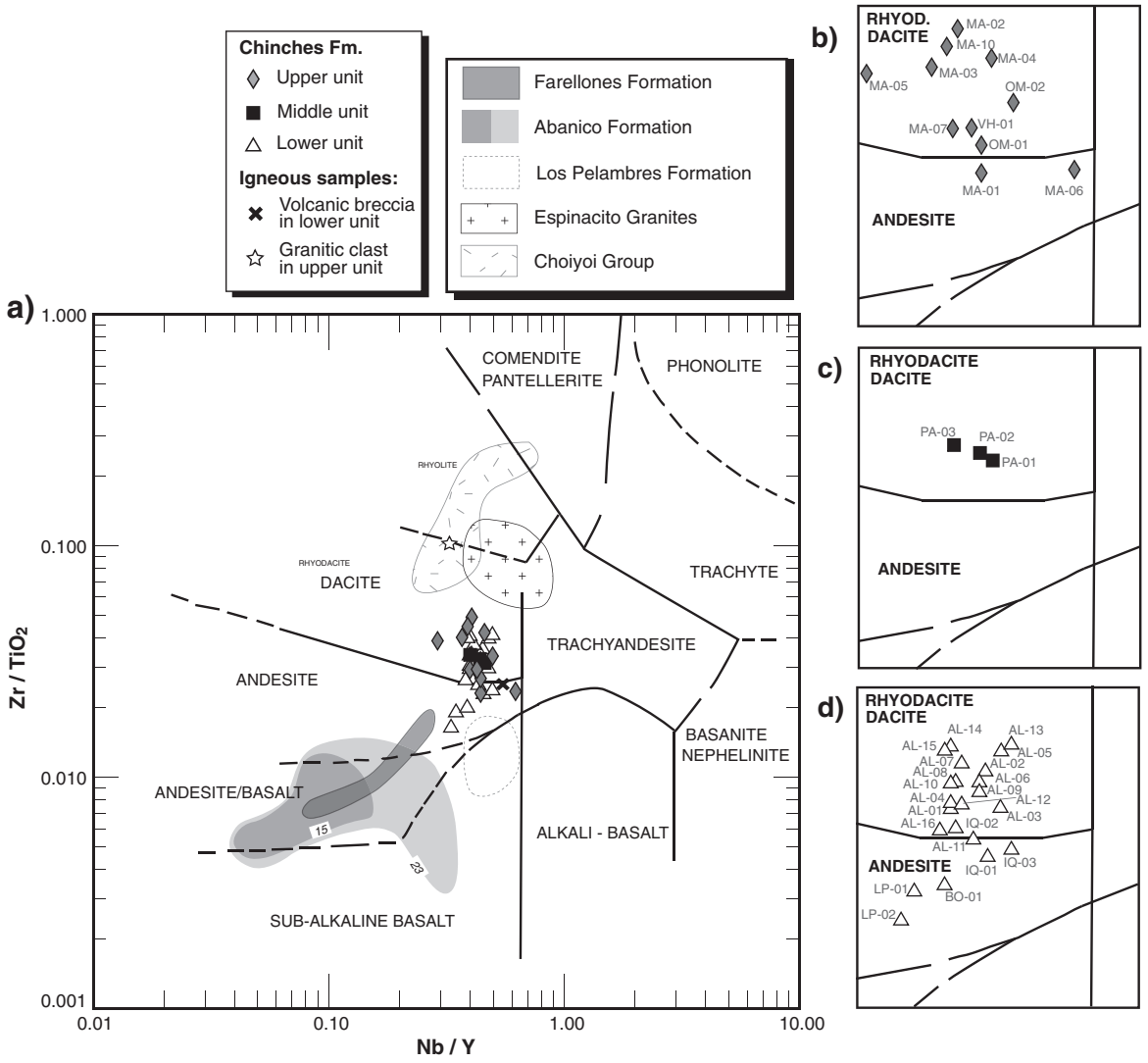

Fig. 14. a) Discrimination of igneous affinity in sedimentary rocks by trace elements plotted on $\log(Zr/TiO_2)$ vs. $\log(Nb/Y)$ diagram (minor elements Zr, Nb and Y in ppm and TiO_2 wt.%*10,000) (after Winchester and Floyd, 1977). b–d) Magnification of the diagram in Fig. 14a, including the stratigraphic units. The gray areas for the Abanico Formation indicate the cumulative frequency curves (percentages are indicated).

plagioclase in the lower and middle units compared to the basal parts of the succession (Fig. 5). Moreover, considering that samples of these strata have an intermediate affinity between basic and acidic (Figs. 14 and 15) we suggest that the origin corresponds to a mixture of sources, possibly the Farellones Formation and rocks from the acidic volcanic rocks of the Choiyoi Group. Pérez (2001) did not consider this strong signal rhyolitic material at lower strata of the Chinches Formation (Fig. 16) for his paleogeographic interpretation. This stage of provenance, represented by the lower and middle units of the Chinches Formation, can be assigned to the Early to Middle Miocene (ca. 19–12.5 Ma, Fig. 4) according to the geochronological data of Jordan et al. (1996).

6.5.3. Third stage: acidic igneous source

The final stage of the basin provenance is characterized by arkosic and rhyodacitic tendencies of the samples from the highest part of the upper unit based on the (Na_2O/K_2O), (SiO_2/Al_2O_3) and (Zr/TiO_2) ratios (Figs. 9 and 14), which indicate that its source was mainly acidic igneous material, probably rhyolitic and/or granitic. The potential source of this material would correspond to the acidic rocks of the Espinacito Granites and the Choiyoi Group, which are geochemically well related to the sediments of the upper unit of the Chinches Formation (Figs. 13a and 15). This third stage of provenance, represented by the upper unit of the Chinches Formation, is assigned to the Late Miocene (ca. 12.5–10 Ma) after fission-track data of Jordan et al. (1996). Particularly, some samples (MA-06 and MA-07) also register a local supply from a tuffaceous unit at this stage, that could be related to the La Ramada Volcanic Complex; this complex is well related in age (12.7 ± 0.6 Ma–10.7 ± 0.7 Ma) to the upper unit of the Chinches Formation (Fig. 4), but does not register tuffs in its description (Pérez, 1995).

7. Conclusive remarks

7.1. Evolution of the tectonically uplifted blocks

The provenance study on the Chinches Formation presented above allows us to define a clear progression of three pulses of tectonic uplift (19 Ma, 10–12.5 Ma, 12.5–10.5 Ma, Figs. 1c and 4) of the La Ramada Fold-and-thrust Belt, whose blocks contributed to the Manantiales Basin during the Miocene. In the first stage of the basin's development (ca. 19 Ma), the main contribution probably came from andesitic rocks of the Farellones Formation in the Principal Cordillera. The structural model of Cristallini et al. (1994) also shows an uplift of the Principal Cordillera at a similar age, producing a thin-skinned and east-vergent fold-

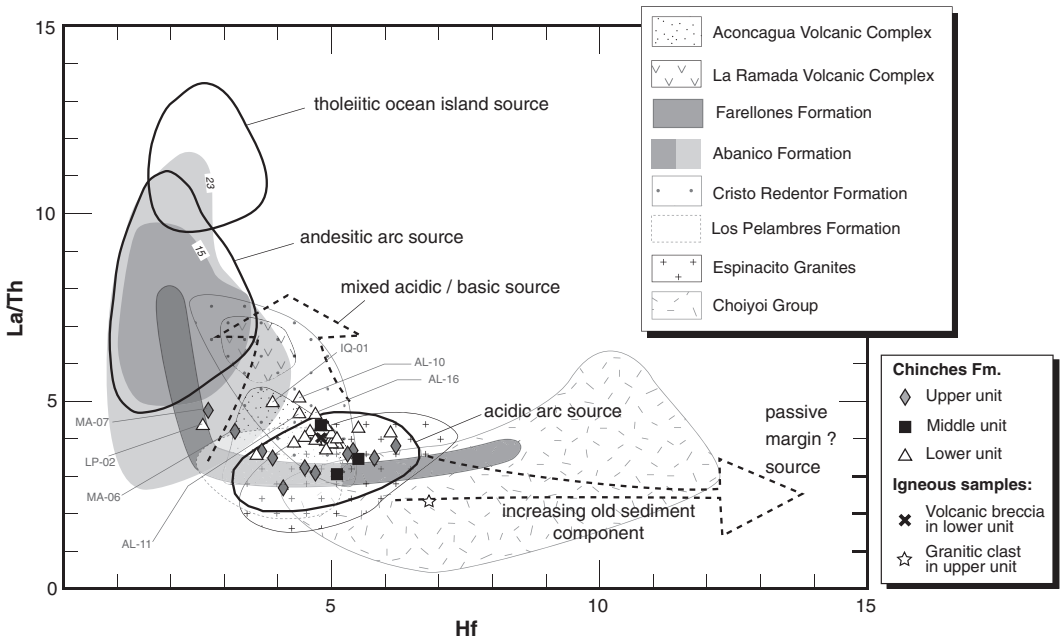

Fig. 15. La/Th vs. Hf proposed for turbiditic sandstones (elements in ppm) (after Floyd and Leveridge, 1987; based on Taylor and McLennan, 1985, among others). The gray areas for the Abanico Formation indicate the cumulative frequency curves (percentages are indicated). We show a trend from a mixed acidic/basic source to an acidic source with a gray translucent arrow.

and-thrust belt. This structure also includes Mesozoic rocks, which contributed to the filling of the Manantiales Basin during all of its evolution. The second stage (ca. 19–12.5 Ma) of the provenance model shows a new source, the Choiyoi Group, contributing to the basin fill, indicating that the Frontal Cordillera (Cordón del Espinacito) at these latitudes was a topographic high in an early stage of the basin evolution. This stage would be related to a major structural change of the La Ramada Fold-and-thrust Belt from a thin- to a thick-skinned configuration, that Cristallini et al. (1994) and Cristallini and Ramos (2000) related to tectonic inversion of Triassic normal faults. The third stage (ca. 12.5–10.5 Ma) has a source with a strong acidic character in the upper unit of the succession, suggesting that the Frontal Cordillera at its outcrops in Cordón del Espinacito, formed by acidic rocks of the Choiyoi Group and the Espinacito Granites, became an important area of supply to the Chinches Formation during its last stage of development.

7.2. The tectonic implications of the provenance progression

Our work shows a clear progression from intermediate igneous sources in the lower unit towards more acidic sources in the upper unit of the Chinches Formation, without repetition of sequences within the full succession. Thus, sedimentation was continuous for nearly the entire 4 km thickness of the Manantiales Basin as was proposed by Jordan et al. (1996) and different from what was proposed by Pérez (1995, 2001). The significance of this result is related to the syntectonic character of such a thick succession, which has registered three major pulses associated with the uplift of the Andes at these latitudes. The consideration of a repeated sequence within the Chinches Formation led Pérez (2001) to interpret a complex depositional relationship of the members that he recognized in the formation and to postulate a late beginning of the uprising of the Frontal Cordillera. We clearly link the first stage of development of the contribution Manantiales Basin to the supply of Miocene volcanism in the Principal Cordillera (Farellones Formation), which decreased progressively in the studied sedimentary succession, leading to an input source area dominated by the Cordón del Espinacito block (Choiyoi Group and Espinacito Granites). Our data and analysis show that the rise of this block began at ca. 19 Ma, earlier than proposed by Pérez (2001) (ca. 10 Ma). Moreover, previous structural studies at this latitude by Cristallini et al. (1994, 1996) and Cristallini and Ramos (2000) did not establish clearly the timing of this event of deformation, with suggested ages between the Early Miocene (20 Ma) to the Pliocene. Thus, our result is significant for the history of the Andes since the uprising of the Cordón del Espinacito block represents the beginning of the thick-skinned tectonics of the La Ramada Fold-and-thrust Belt, after thin-skinned tectonics, and that is related to the flattening of the subduction slab at these latitudes of the Andes.

For 30°S, Kay et al. (1987, 1991) proposed that the shallowing of the subduction zone began at ca. 18 Ma, evidenced by high-angle reverse faulting indicating a thickening of the crust, and the intrusion of andesitic subvolcanic plutons and porphyritic stocks (ca. 16–15 Ma, Maksaev et al., 1984; Bissig et al., 2000, 2001). They also show that andesitic volcanism decreased markedly (ca. 16–11 Ma) and deformation and igneous activity propagated eastward since ca. 18 Ma. For the same latitude, Bissig et al. (2002) defined three pediplains of regional extent, ca. 17–15 Ma, 14–12.5 Ma and 10–6 Ma, related to uplift events associated with the development of the flat-slab (Bissig, 2001). By the other hand, Yáñez et al. (2001) proposed that the cause of the flattening of the slab was the subduction of the Juan Fernández Ridge. The effect of this ridge would have arrived at 32°–33°S between ca. 12 and 10 Ma (Kay and Mpodozis, 2002). Our study indicates that the thick-skinned tectonics at these latitudes began at ca. 19 Ma, with an uplift peak at ca. 12.5–10 Ma. Thus, we propose that the shallowing of the slab started at ca. 19 Ma similar to that at 30°S, and the arrival of the Juan Fernández Ridge at ca. 12–10 Ma is related to the flattening climax of the subduction zone that produced the principal migration of deformation and magmatism to the east.

Acknowledgments

We are grateful for funding by Fondecyt Project No 1090165 (Luisa Pinto), funded by Comisión Nacional de Investigación Científica y Tecnológica (CONICYT). Significant support was obtained from the IGCP Project No 586Y, funded by UNESCO, that supported the field

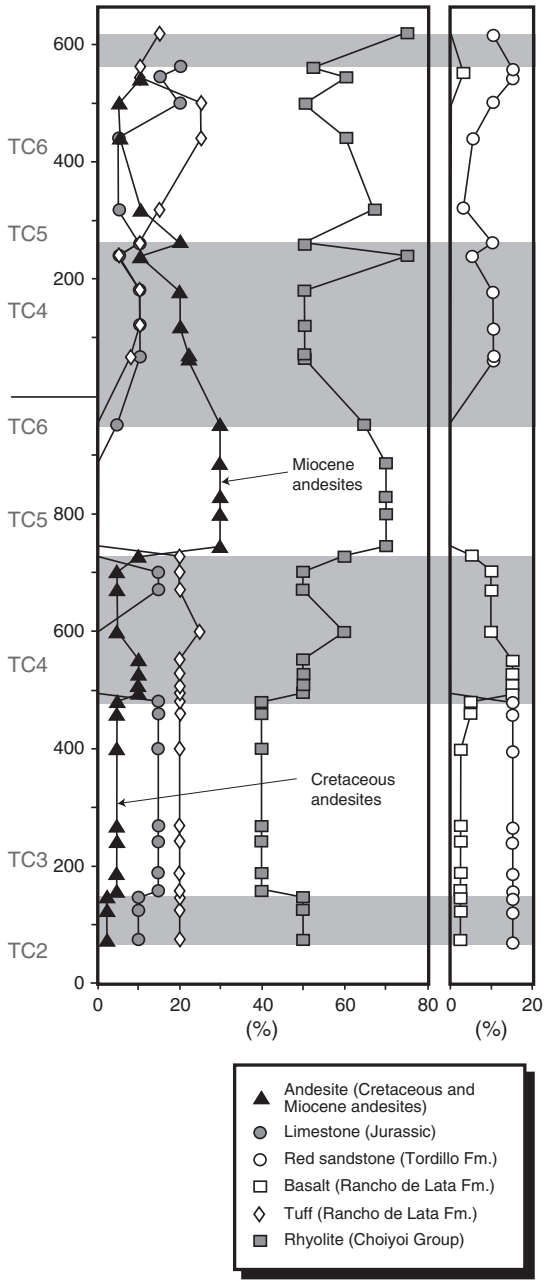

Fig. 16. Petrology of sedimentary clasts of the Chinches Formation based on Pérez (2001). The lithology of the source rocks is indicated for each sample. We have considered the two studied columns of Pérez (2001) from the Aldeco River as a single column, without a repetition of the succession. Tc1 to Tc6 are the members of the Chinches Formation defined by Pérez (1995, 2001). There are no GPS references to correlate this column to ours.

trips and scientific meetings, which helped us to improve our interpretations. We also appreciate the support given by the Geology Department of the University of Chile. Important scientific contributions were made through collaborations with A. Morton (HM Research, Associates, United Kingdom), B. Moine (CNRS, France), G. Hoke (Syracuse University, United States), L. Giambiagi (CONICET, Argentina) and T. Aldunate (University of Chile). Finally, we appreciate the technical assistance provided by J. Vargas (University of Chile), M. Olivera of Don Lisandro (Barreal, Argentina) and we would like to thank the staff at X-Strata (La Junta, Argentina) for their logistical support in the field campaigns. Careful reviews by L. Aguirre, J. Le Roux, S. Herrera (University of Chile), J. Fodick (Indiana University) and S. Mullin helped to greatly improve the manuscript.

References

Álvarez, P.P., Pérez, D.J., 1993. Estratigrafía y estructura de las nacientes del río Colorado, Alta cordillera de San Juan. In: Ramos, V.A. (Ed.), XII Congreso Geológico Argentino y II Congreso de Exploración de Hidrocarburos. Actas II, pp. 78–84.
Arribas, J., Critelli, S., Johnsson, M.J. (Eds.), 2007. Sedimentary provenance and petrogenesis: perspectives from petrography and geochemistry. Special Paper Geological Society of America 420 (396 pp.).
Aubouin, J., 1973. Des tectoniques superposées et de leur signification par rapport aux modèles géophysiques: l'exemple der, Dinarides: paléotectonique, tectonique, tarditectonique, néotectonique. Bull. Soc. Géol. Fr. 15 (7), 426–460.
Baranzangi, M., Isacks, B.L., 1976. Spatial distribution of earthquakes and subduction of the Nazca plate beneath South America. Geology 4, 686–692.
Bhatia, M.R., Taylor, S.R., 1981. Trace-element geochemistry and sedimentary provinces: a study from the Tasman geosyncline, Australia. Chem. Geol. 33, 115–125.
Bhatia, M., 1983. Plate tectonics and geochemical composition of sandstones. J. Geol. 91, 611–627.
Bissig, T., 2001. Metallogenesis of the Miocene El Indio-Pascua goldsilver-copper belt, Chile/Argentina: geodynamic, geomorphological and petrochemical controls on epithermal mineralization. Unpublished Ph.D. Thesis, Queen's University, Kingston, Canada, 531 pp.
Bissig, T., Clark, A.H., Lee, J.K.W., Heather, K.B., 2000. Revised metallogenetic model for the El Indio-Pascua/Lama Au (-Ag, Cu) belt, Regiones III/IV, Chile, Provincia San Juan, Argentina. GSA Annual Meeting, Reno Nevada, Abstracts with Programs A-280.
Bissig, T., Lee, J.K.W., Clark, A.H., Heather, K.B., 2001. The Cenozoic history of magmatic activity and hydrothermal alteration in the Central Andean flat-slab region: new 40Ar–39Ar constraints from the El Indio-Pascua Au (-Ag, Cu) belt, 298200-308300S. Int. Geol. Rev. 41, 312–340.
Bissig, T., Clark, A.H., Lee, J.K.W., Hodgson, C.J., 2002. Miocene landscape evolution in the Chilean flat-slab transect: uplift history and geomorphologic controls on epithermal processes in the El Indio-Pascua Au (-Ag, Cu) belt. Econ. Geol. 97, 971–996.
Bissig, T., Clarck, A.H., Lee, J.K.W., von Quadt, A., 2003. Petrogenetic and metallogenetic responses to Miocene slab flattening: new constrains from the El Indio-Pascua Au–Ag–Cu belt, Chile/Argentina. Mineral. Deposita 38, 844–862.
Cahill, T., Isacks, B.L., 1992. Seismicity and shape of the subducted Nazca Plate. J. Geophys. Res. 97, 17503–17529.
Charrier, R., Baeza, O., Elgueta, S., Flynn, J.J., Gans, P., Kay, S.M., Muñoz, N., Wyss, A.R., Zurita, E., 2002. Evidence for Cenozoic extensional basin development and tectonic inversion south of the flat-slab segment, southern Central Andes, Chile (33°–36°S.L.). J. S. Am. Earth Sci. 15 (1), 117–139.
Charrier, R., Bustamante, M., Comte, D., Elgueta, S., Flynn, J.J., Iturra, N., Muñoz, N., Pardo, M., Thiele, R., Wyss, A.R., 2005. The Abanico extensional basin: regional extension, chronology of tectonic inversion and relation to shallow seismic activity and Andean uplift. N. Jb. Geol. Paläont. (Abh.) 236, 43–77.
Charrier, R., Pinto, L., Rodríguez, M.P., 2007. Tectonostratigraphic evolution of the Andean orogen in Chile. In: Moreno, T., Gibbons, W. (Eds.), The Geology of Chile. The Geological Society of London, Special Publication, UK, chapter 3, pp. 21–114.
Cox, K.G., Bell, J.D., Pankhurst, R.J., 1979. The Interpretation of Igneous Rocks. George Allen & Unwin 450 pp.
Cristallini, E.O., Cangini, A.H., 1993. Estratigrafía y estructuras las nacientes del río Volcán, Alta Cordillera de San Juan. XII Congreso Geológico Argentino and II Congreso de Exploración de Hidrocarburos. 3, pp. 85–92 (Buenos Aires).
Cristallini, E.O., Ramos, V.A., 2000. Thick-skinned and thin-skinned thrusting in La Ramada fold and thrust belt. Crustal evolution of the High Andes of San Juan, Argentina (32° SL). Tectonophysics 317, 205–235.
Cristallini, E.O., Mosquera, A., Ramos, V.A., 1994. Estructura de la Alta Cordillera de San Juan. Rev. Asoc. Geol. Argent. 49 (1–2), 165–183.
De La Roche, H., 1968. Comportement géochimique différentiel de Na, K et Al dans les formations volcaniques et sédimentaires. Un guide pour l'étude des formations métamorphiques et plutoniques. C. R. Acad. Sci. Fr. 267 (D), 39–42.
Dewey, J.F., Bird, J.M., 1970. Mountain belts and the new global tectonics. J. Geophys. Res. 75 (14), 2625–2647.
Dickinson, W., 1970. Interpreting detrital modes of graywacke and arkose. J. Sediment. Petrol. 40, 695–707.
Dickinson, W.R., Beard, L.S., Brakenridge, G.R., Erjavee, J.R., Ferguson, R.C., Inman, K.F., 1983. Provenance of North American Phanerozoic sandstones in relation to plate tectonic setting. Geol. Soc. Am. Bull. 94, 222–235.
Einsele, G., 1992. Sedimentary Basins: Evolution, Facies and Sediment Budget. Springer-Verlag, Berlin Heidelberg, Germany (632 pp.).
Fedo, C.M., Nesbitt, H.W., Young, G.M., 1995. Unraveling the effects of potassium metasomatism in sedimentary rocks and Paleosols, with implications for paleoweathering conditions and provenance. Geology 23, 921–924.
Floyd, P.A., Leveridge, B.E., 1987. Tectonic environment of the Devonian Gramscatho basin, south Cornwall: framework mode and geochemical evidence from turbiditic sandstones. J. Geol. Soc. Lond. 144, 531–542.
Fock, A., Charrier, R., Farías, M., Muñoz, M., 2006. Fallas de vergencia oeste en la Cordillera Principal de Chile Central: Inversión de la cuenca de Abanico (33°–34°S). Revista de la Asociación Geológica Argentina, special publication 6, pp. 48–55.
Folk, R., Andrews, P., Lewis, D., 1970. Detrital sedimentary rock classification and nomenclature for use in New Zealand. N. Z. J. Geol. Geophys. 13, 937–968.
Fuentes, F., 2004. Petrología y metamorfismo de muy bajo grado de unidades volcánicas oligoceno-miocenas en la ladera occidental de Los Andes de Chile Central (33°S). Ph.D. Thesis (Unpublished), Universidad de Chile, 403 pp.
Gabo, J.S.A., Dimalanta, C.B., Asio, M.G.S., Queaño, K.L., Yumul Jr., G.P., Imai, A., 2009. Geology and geochemistry of the clastic sequences from Northwestern Panay

(Philippines): implications for provenance and geotectonic setting. Tectonophysics 479, 111–119. http://dx.doi.org/10.1016/j.tecto.2009.02.004.
Giambiagi, L.B., Ramos, V.A., Godoy, E., Álvarez, P.P., Orts, S., 2003a. Cenozoic deformation and tectonic style of the Andes, between 33° and 34° South Latitude. Tectonics 22 (4), 1041. http://dx.doi.org/10.1029/2001TC001354 (pp. 15–1-15–18).
Giambiagi, L.B., Álvarez, P.P., Godoy, E., Ramos, V.A., 2003b. The control of pre-existing extensional structures in the evolution of the southern sector of the Aconcagua fold and thrust belt. Tectonophysics 369, 1–19.
Gutscher, M.A., 2002. Andean subduction and their effect on the thermal structure and interpolate coupling. J. S. Am. Earth Sci. 15, 3–10.
Gutscher, M.A., Spakman, W., Bkjwaard, H., Engdahl, E.R., 2000. Geodynamics of flat subduction: seismicity and tomographic constraints from the Andean margin. Tectonics 19, 814–833.
Herron, M.M., 1988. Geochemical classification of terrigenous sands and shales from core or log data. J. Sediment. Petrol. 58, 820–829.
Hofer, G., Wagreich, M., Neuhuber, S., 2013. Geochemistry of fine-grained sediments of the upper Cretaceous to Paleogene Gosau Group (Austria, Slovakia): implications for paleoenvironmental and provenance studies. Geosci. Front. 4, 449–468.
Ingersoll, R.V., Bullard, T.F., Ford, R.L., Grimm, J.P., Pickle, J.D., Sares, S.W., 1984. The effect of grain size on detrital modes: a test of the Gazzi-Dickinson point-counting method. J. Sediment. Petrol. 54, 103–116.
Jara, P., Charrier, R., 2011. Perfil estructural en la Alta Cordillera de Chile central a 32º15'S. XVIII Congreso Geológico Argentino, Neuquén, Sesión S12, p. 2.
Jara, P., Charrier, R., 2014. Nuevos antecedentes estratigráficos y geocronológicos para el Meso-Cenozoico de la Cordillera Principal de Chile entre 32° y 32°30'S. Implicancias estructurales y paleogeográficas. Andean Geol. 41 (1), 174–209. http://dx.doi.org/10.5027/andgeoV41n1-a07.
Jordan, T.E., Isacks, B.L., Allmendinger, R.W., Brewer, J.A., Ramos, V.A., Ando, C.J., 1983. Andean tectonics related to geometry of subducted Nazca Plate. Geol. Soc. Am. Bull. 94, 341–361.
Jordan, T.E., Tamm, V., Figueroa, G., Flemings, P.B., Richards, D., Tabbutt, K., Cheatham, T., 1996. Development of the Miocene Manantiales foreland basin, Principal Cordillera, San Juan, Argentina. Rev. Geol. Chile 23 (1), 43–79.
Jorge, R.C.G.S., Fernandes, P., Rodrigues, B., Pereira, Z., Oliveira, J.T., 2013. Geochemistry and provenance of the Carboniferous Baixo Alentejo Flysch Group, South Portuguese Zone. Sed. Geol. 284–285, 133–148.
Kay, S.M., Mpodozis, C., 2002. Magmatism as a probe to the Neogene shallowing of the Nazca plate beneath the modern Chilean flat-slab. J. S. Am. Earth Sci. 15 (1), 39–57.
Kay, S.M., Maksaev, V., Moscoso, R., Mpodozis, C., Nasi, C., Gordillo, C.E., 1987. Tertiary Andean magmatism in Chile and Argentina between 28°S and 33°S: correlation of magmatic chemistry with a changing Benioff zone. J. S. Am. Earth Sci. 1 (1), 21–38.
Kay, S.M., Mpodozis, C., Ramos, V.A., Munizaga, F., 1991. Magma source variations for Tertiary magmatic rocks associated with a shallowing subduction zone and a thickening crust in the Central Andes (28 ° to 33°S). In: Harmon, R.S., Rapela, C.W. (Eds.), Andean Magmatism and its Tectonic Setting. Geological Society of America, Special Paper 265, pp. 113–137.
Kley, J., Monaldi, C.R., Salfity, J.A., 1999. Along-strike segmentation of the Andean foreland: causes and consequences. Tectonophysics 301, 75–94.
Krawinkel, H., Wozazek, S., Krawinkel, J., Hellmann, W., 1999. Heavy-mineral analysis and clinopyroxene geochemistry applied to provenance analysis of lithic sandstones from the Azuero-Soná Complex (NW Panama). Sed. Geol. 124, 149–168.
Kuno, H., 1968. Differentiation of basalt magmas. In: Hess, H.H., Poldervaart, A.A. (Eds.), Basalts: The Poldervaart Treatise on Rocks of Basaltic Composition 2. Interscience, New York, pp. 623–688.
Kutterolf, S., Diener, R., Schacht, U., Krawinkel, H., 2008. Provenance of the Carboniferous Hochwipfel Formation (Karawanken Mountains, Austria/Slovenia) — geochemistry versus petrography. Sed. Geol. 203, 246–266.
Le Maitre, R.W., Bateman, P., Dudek, A., Keller, J., Lameyre, J., Le Bas, M.J., Sabine, P.A., Schmid, R., Sorensen, H., Streckeisen, A., Woolley, A.R., Zanettin, B., 1989. A Classification of Igneous Rocks and Glossary of Terms: Recommendations of the International Union of Geological Sciences Subcommission on the Systematics of Igneous Rocks. Blackwell Scientific, Oxford (193 pp.).
Lee, Y., 2002. Provenance derived from the geochemistry of late Paleozoic–early Mesozoic mudrocks of the Pyeongan Supergroup, Korea. Sed. Geol. 149 (4), 219–235.
Levi, B., 2010. Non published Geochemical Data of Various Units Were Provided by Luis Aguirre (Universidad de Chile) From a Study Realized by Beatriz Levi (Stockholm University).
Maksaev, V., Moscoso, R., Mpodozis, C., Nasi, C., 1984. Las unidades volcánicas y plutónicas del cenozoico superior en la Alta Cordillera del Norte Chico (29°–31°S): Geología, alteración hidrothermal y mineralización. Rev. Geol. Chile (Andean Geol.) 21, 11–51.
Mange, M.A., Maurer, H.F.W., 1992. Heavy Minerals in Colour. Chapman and Hall, London (147 pp.).
Mange, M.A., Morton, A.C., 2007. Geochemistry of heavy minerals. In: Mange, M., Wright, D.K. (Eds.), Heavy Minerals In Use. Developments in Sedimentology 58, pp. 345–391.
Martínez, A., 2005. Secuencias volcánicas permo-triásicas de los cordones del Portillo y del Plata, Cordillera Frontal, Mendoza: su interpretación tectónica. Ph.D. Thesis (Unpublished), Universidad de Buenos Aires, Facultad de Ciencias Exactas y Naturales, Departamento de Ciencias Geológicas, 274 pp.
Martínez, A., Giambiagi, L., 2010. Evolución petrológica y geoquímica del magmatismo bimodal Permo-Triásico del Grupo Choiyoi en el cordón del Portillo, Mendoza, Argentina. Trabajos de Geología, Oviedo 30, pp. 432–451.
McLennan, S.M., Bock, B., Hemming, S.R., Hurowitz, J.A., Lev, S.M., McDaniel, D.K., 2004. The roles of provenance and sedimentary processes in the geochemistry of sedimentary rocks. In: Lentz, D.R. (Ed.), Geochemistry of Sediments and Sedimentary Rocks: Evolutionary Considerations to Mineral Deposit-Forming Environments. Geological Association of Canada, GeoText vol. 4, pp. 7–38.
Mirré, J.C., 1966. Geología del valle del Río de Los Patos (entre Barreal y Las Hornillas). Rev. Asoc. Geol. Argent. 21 (4), 211–231.
Moine, B., 1974. Caractères de sédimentation et de métamorphisme des séries précambriennes épizonales à catazonales du centre de Madagascar (Région d'Ambatofinandrahana) (Ph.D. Thesis) Mémoire 31. Université de Nancy, Fr. (293 pp.).
Montecinos, P.R., 2008. Edad y petrogénesis del magmatismo Oligoceno-Mioceno de los Andes de Chile central a los 33°S: implicación geodinámica para el margen de América del Sur. Ph.D. Thesis (Unpublished), Departamento de Geología, Universidad de Chile, 159 pp.
Morton, A.C., 1991. Geochemical studies of detrital heavy minerals and their application to provenance studies. In: Morton, A., Todd, S., Haughton, P. (Eds.), Developments in Sedimentary Provenance Studies. J. Geol. Soc. Lond., Special Publication 57, pp. 31–45.
Mpodozis, C., Ramos, V.A., 1989. The Andes of Chile and Argentina. In: Ericksen, G.E., Cañas Pinochet, M.T., Reinemund, J.A. (Eds.), Geology of the Andes and its Relation to Hydrocarbon and Mineral Resources. Circum-Pacific Council for Energy and Mineral Resources. Earth Science Series 11, pp. 59–90.
Mpodozis, C., Brockway, H., Marquardt, C., Perelló, J., 2009. Geocronología U/Pb y tectónica de la región Los Pelambres-Cerro Mercedario: Implicancias para la evolución cenozoica de los Andes del centro de Chile y Argentina. XII Congreso Geológico Chileno, Santiago, Chile (S9–059.
Munizaga, F., Vicente, J.C., 1982. Acerca de la zonación plutónica y del volcanismo miocénico en los Andes de Aconcagua (Lat. 32–33°S): datos radiométricos K–Ar. Revista Geológica de Chile, No. 16, pp. 3–21.
Muñoz Sáez, C., Pinto, L., Charrier, R., Nalpas, T., 2014. Importance of volcanic load and shortcut fault development during inversion of an Eocene-Oligocene extensional basin in the Andes: the Abanico Basin case, Central Chile (33°–35°S). Andean Geol. 41 (1), 1–28. http://dx.doi.org/10.5027/andgeoV41n1-a01.
Nesbitt, H., Young, G., 1982. Early Proterozoic climates and plate motions inferred from major elements chemistry of lutites. Nature 299, 715–717.
Nesbitt, H.W., Young, G.M., 1984. Prediction of some weathering trends of plutonic and volcanic rocks based on thermodynamic and kinetic considerations. Geochim. Cosmochim. Acta 48, 1523–1534.
Parfenoff, A., Pomerol, Ch., Tourenq, J., 1970. Les minéraux lourds en grains. Méthodes d'étude et Détermination. Masson, Paris (571 pp.).
Pearce, J.A., 1983. Role of the subcontinental lithosphere in magma genesis at active continental margins. In: Hawkesworth, C.J., Norry, M.J. (Eds.), Continental Basalts and Mantle Xenoliths. Shiva Publishing, Nantwich, pp. 230–249.
Pearce, J.A., Cann, J.R., 1973. Tectonic setting of basic volcanic rocks determined using trace element analyses. Earth Planet. Sci. Lett. 19, 290–300.
Pérez, D.J., 1995. Estudio geológico del Cordón del Espinacito y regiones adyacentes, provincial de San Juan. Universidad de Buenos Aires. Ph.D. Thesis (Unpublished), Buenos Aires, 262 pp.
Pérez, D.J., 2001. Tectonic and unroofing history of Neogene Manantiales foreland basin deposits, Cordillera Frontal (32°30′S), San Juan Province, Argentina. J. S. Am. Earth Sci. 14, 693–705.
Pérez, D.J., Ramos, V.A., 1996. Los depósitos sinorogénicos. Geología de la Región del Aconcagua, Provincias de San Juan y Mendoza, Subsecretaría de Minería de la Nación, Dirección del Servicio Geológico, Buenos Aires. In: Ramos, et al. (Eds.), Anales 24(11), pp. 317–341.
Pettijohn, F., Potter, P., Siever, R., 1972. Sand and Sandstones. Springer-Verlag, New York.
Pettijohn, F.J., Potter, P.E., Siever, R., 1987. Sand and Sandstone. Springer, New York (553 pp.).
Pinto, L., Hérail, G., Moine, B., Fontan, F., Charrier, R., Dupré, B., 2004. Using geochemistry to establish the igneous provenances of the Neogene continental sedimentary rocks in the Central Depression and Altiplano, Central Andes. Sed. Geol. 166 (1/2), 157–183.
Pinto, L., Hérail, G., Montan, F., de Parseval, Ph., 2007. Neogene erosion and uplift of the western edge of the Andean Plateau as determined by detrital heavy mineral analysis. Sed. Geol. 195, 217–237.
Pinto, L., Alarcón, P., Jara, P., Baeza, S., 2014n. Relation Between Volcanic Units in the Principal Cordillera Chile–Argentina 32°–33°S: New Evidence for a Stratigraphic Redefinition Through Petrography and Geochemistry, (in preparation).
Potter, P.E., 1978. Petrology and chemistry of modern big river sands. J. Geol. 86, 423–449.
Ramos, V.A., 1999. Los depósitos sinorogénicos terciarios de la Región Andina. In: Caminos, R. (Ed.), Geología Argentina. Subsecretaría de Instituto de Geología y Recursos Minerales, Buenos Aires. Anales 29 (22), pp. 651–682.
Ramos, V.A., Cegarra, M.I., Cristallini, E., 1996a. Cenozoic tectonics of the high Andes of west-central Argentina (30–36°S latitude). Tectonophysics 259, 185–200.
Ramos, V.A., Aguirre-Urreta, M.B., Alvarez, P., Cegarra, M.I., Cristallini, E.O., Kay, S.M., Lo Forte, G.L., Pereyra, F.X., Pérez, D.J., 1996b. Geología de la Región del Aconcagua, Provincias de San Juan y Mendoza, Subsecretaría de Minería de la Nación, Dirección del Servicio Geológico, Buenos Aires. Anales 24 (510 pp.).
Ramos, V.A., Cristallini, E., Pérez, D.J., 2002. The Pampean flat-slab of the Central Andes. J. S. Am. Earth Sci. 15, 59–78.
Rivano, S., Sepúlveda, P., Boric, R., Espiñeira, D., 1993. Hojas Quillota y Portillo, V Región. Servicio Nacional de Geología y Minería, Carta Geológica de Chile, N° 73.
Rodríguez, M.P., Pinto, L., Encinas, A., 2012. Neogene erosion and relief evolution in Central Chile forearc (33–34°S) as determined by detrital heavy mineral analysis. Geol. Soc. Am. Spec. Pap. 487, 141–162. http://dx.doi.org/10.1130/2012.2487(09).
Rollinson, H.R., 1993. Using Geochemical Data: Evaluation, Presentation, Interpretation. Longman, U.K. (352 pp.)

Roser, B., Korsch, R., 1986. Determination of tectonic setting of sandstone-mudstone suites using SiO2 content and K2O/Na2O ratio. J. Geol. 94, 635–650.
Rudnick, R.L., Gao, S., 2004. Composition of the continental crust. In: Rudnick, R.L. (Ed.), The Crust: Treatise on Geochemistry. Elsevier-Pergamon, Oxford, pp. 1–64.
Sernageomin, 2003. Mapa Geológico de Chile, 1:1.000.000. Servicio Nacional de Geología y Minería.
Stipanicic, P.N., Rodrigo, F., Baulíes, O.L., Martínez, C.G., 1968. Las formaciones presenonianas en el denominado Macizo Nordpatagónico y regiones adyacentes. Revista de la Asociación Geológica Argentina 23 (2), 67–98.
Sun, S.S., McDonough, W.F., 1989. Chemical and isotopic systematics of oceanic basalts: implications for mantle composition and processes. In: Saunders, A.D., Norry, M.J. (Eds.), Magmatism in the Ocean Basins: Geological Society, Special Publication, pp. 333–347.
Tassara, A., Yáñez, G., 1996. Thermomechanic segmentation of the Andes (15°–508°S): a flexural analysis approach. In: IRD (Ed.), III International Symposium on Andean Geodynamics (ISAG), St. Malo, France, pp. 115–118.
Taylor, S.R., McLennan, S.M., 1985. The Continental Crust: Its Composition and Evolution. Blackwell Scientific Publications, Oxford (312 pp.).
Taylor, S.R., Ewart, A., Capp, A.C., 1968. Leucogranites and rhyolites: trace element evidence for fractional crystallization and partial melting. Lithos 1, 179–186.
Vergara, M., Nyström, J., 1996. Geochemical features of Lower Cretaceous back-arc lavas in the Andean Cordillera, Central Chile (31–34°S). Rev. Geol. Chile 23 (1), 97–106.
Vergara, M., Rivano, S., Anex, P., 1993. Características geoquímicas de las rocas volcánicas de la Formación Los Pelambres, Cordillera Principal (31°–32°S). Estudio Preliminar. XII Congreso Geológico Argentino and II Congreso de exploración de Hidrocarburos, Buenos Aires vol. 4, pp. 166–170.
Winchester, J., Floyd, P., 1977. Geochemical discrimination of different magma series and their differentiation products using immobile elements. Chem. Geol. 20, 325–343.
Yáñez, G.A., Ranero, C.R., Von Huene, R., Díaz, J., 2001. Magnetic anomaly interpretation across the southern central Andes (32°–34°S): the role of the Juan Fernández Ridge in the late Tertiary evolution of the margin. J. Geophys. Res. 106 (B4), 6325–6345.
Yang, X., He, D., Wang, Q., Tang, Y., Tao, H., Li, D., 2011. Provenance and tectonic setting of the Carboniferous sedimentary rocks of the East Junggar Basin, China: evidence from geochemistry and U–Pb zircon geochronology. Gondwana Res. 22, 567–584.